Article

Cell Reports

Heat Shock Factor 2 Protects against Proteotoxicity by Maintaining Cell-Cell Adhesion

Graphical Abstract

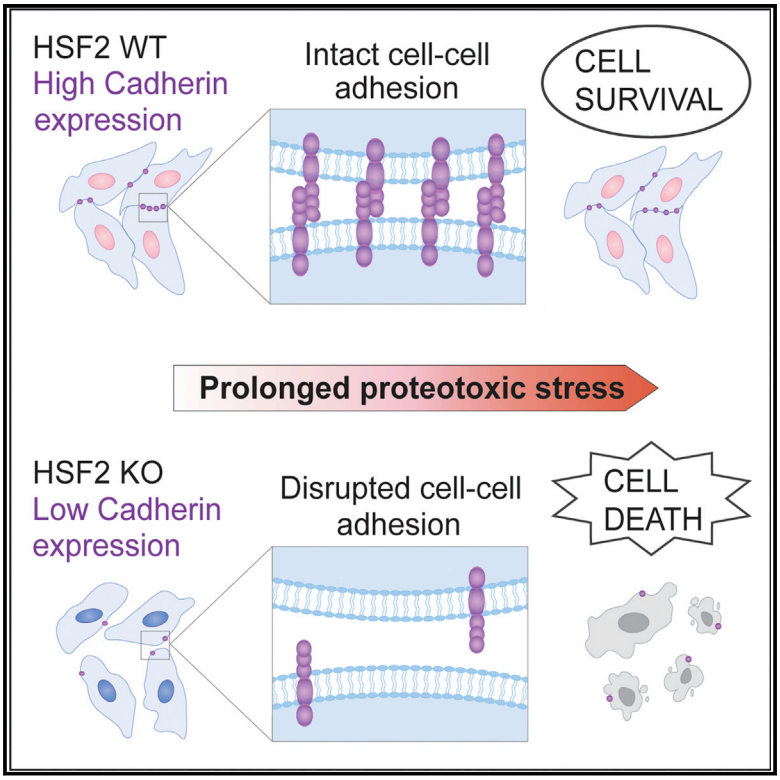

Authors

Jenny Joutsen, Alejandro Jose Da Silva, Jens Christian Luoto, ..., Délara Sabéran-Djoneidi, Eva Henriksson, Lea Sistonen

Correspondence

lea.sistonen@abo.fi

In Brief

Joutsen et al. show that heat shock factor 2 (HSF2) is essential for cell survival during prolonged proteotoxicity. Lack of HSF2 leads to marked misregulation of cadherin superfamily genes and functional impairment of cell-cell adhesion. Cell-cell adhesion is found to be a key determinant of proteotoxic stress resistance.

Highlights

- HSF2 is required to maintain cell-cell adhesion
- HSF2 deficiency leads to downregulation of cadherin superfamily genes
- Impaired cell-cell adhesion sensitizes cells to prolonged proteotoxic stress
- Cadherin-mediated cell-cell adhesion is a survival determinant upon proteotoxicity

Joutsen et al., 2020, Cell Reports *30*, 583–597
January 14, 2020
https://doi.org/10.1016/j.celrep.2019.12.037

CellPress

Cell Reports
Article

Heat Shock Factor 2 Protects against Proteotoxicity by Maintaining Cell-Cell Adhesion

Jenny Joutsen,[1,2,7] Alejandro Jose Da Silva,[1,2,7] Jens Christian Luoto,[1,2] Marek Andrzej Budzynski,[1,2] Anna Serafia Nylund,[1,2] Aurelie de Thonel,[3,4,5] Jean-Paul Concordet,[6] Valérie Mezger,[3,4,5] Délara Sabéran-Djoneidi,[3,4,5] Eva Henriksson,[1,2] and Lea Sistonen[1,2,8,*]

[1]Faculty of Science and Engineering, Cell Biology, Åbo Akademi University, Tykistökatu 6, 20520 Turku, Finland
[2]Turku Bioscience Centre, University of Turku and Åbo Akademi University, Tykistökatu 6, 20520 Turku, Finland
[3]CNRS, UMR 7216 "Epigenetic and Cell Fate," 75250 Paris Cedex 13, France
[4]University of Paris Diderot, Sorbonne Paris Cité, 75250 Paris Cedex 13, France
[5]Département Hospitalo-Universitaire DHU PROTECT, Paris, France
[6]INSERM U1154, CNRS UMR 7196, Muséum National d'Histoire Naturelle, Paris, France
[7]These authors contributed equally
[8]Lead Contact
*Correspondence: lea.sistonen@abo.fi
https://doi.org/10.1016/j.celrep.2019.12.037

SUMMARY

Maintenance of protein homeostasis, through inducible expression of molecular chaperones, is essential for cell survival under protein-damaging conditions. The expression and DNA-binding activity of heat shock factor 2 (HSF2), a member of the heat shock transcription factor family, increase upon exposure to prolonged proteotoxicity. Nevertheless, the specific roles of HSF2 and the global HSF2-dependent gene expression profile during sustained stress have remained unknown. Here, we found that HSF2 is critical for cell survival during prolonged proteotoxicity. Strikingly, our RNA sequencing (RNA-seq) analyses revealed that impaired viability of HSF2-deficient cells is not caused by inadequate induction of molecular chaperones but is due to marked downregulation of cadherin superfamily genes. We demonstrate that HSF2-dependent maintenance of cadherin-mediated cell-cell adhesion is required for protection against stress induced by proteasome inhibition. This study identifies HSF2 as a key regulator of cadherin superfamily genes and defines cell-cell adhesion as a determinant of proteotoxic stress resistance.

INTRODUCTION

The cells in a human body are constantly exposed to environmental stressors, which challenge the maintenance of protein homeostasis, also called proteostasis. To survive insults that disturb proteostasis, cells rely on a selection of protective mechanisms that can be launched upon stress exposures. The heat shock response is a well-conserved stress protective pathway that is induced in response to cytosolic protein damage and mediated by heat shock transcription factors (HSFs; Joutsen and Sistonen, 2019). Upon activation, HSFs oligomerize, accumulate in the nucleus, and bind to their target heat shock elements (HSEs) at multiple genomic loci (Vihervaara et al., 2013, 2017; Mahat et al., 2016). The canonical HSF target genes encode molecular chaperones, such as heat shock proteins (HSPs), which assist in the maintenance of a correct protein folding environment by refolding the misfolded proteins or directing them to protein degradation machineries (Hartl et al., 2011). In addition, HSFs are important in a variety of other physiological and pathological processes and the repertoire of HSF target genes has been shown to extend beyond the HSPs (Hahn et al., 2004; Åkerfelt et al., 2010; Gonsalves et al., 2011; Mendillo et al., 2012; Riva et al., 2012; Björk et al., 2016; Li et al., 2016).

The human genome encodes six HSF family members (HSF1, HSF2, HSF4, HSF5, HSFX, and HSFY), of which HSF1 and HSF2 are the most extensively studied (Joutsen and Sistonen, 2019). Although these factors are homologous in their DNA-binding domains, they share only a few similarities in the tissue expression patterns, regulatory mechanisms, and signals that stimulate their activity (Jaeger et al., 2016; Gomez-Pastor et al., 2018). HSF1 is essential for HSP expression and cell survival under acute stress conditions (Joutsen and Sistonen, 2019). HSF2 is an unstable protein and its expression is highly context dependent, fluctuating in different cell and tissue types (Sarge et al., 1991; Alastalo et al., 1998), developmental stages (Mezger et al., 1994; Rallu et al., 1997), and during the cell cycle (Elsing et al., 2014). Consequently, regulation of HSF2 protein levels has been considered to be the main determinant of its DNA-binding capacity (Mathew et al., 1998; Budzyński and Sistonen, 2017). Interestingly, the DNA-binding activity of HSF2 increases in cells exposed to lactacystin- or MG132-induced proteasome inhibition (Kawazoe et al., 1998; Mathew et al., 1998; Pirkkala et al., 2000), indicating that HSF2 can respond to proteostasis disruption. Nevertheless, the molecular details of the activation mechanisms of HSF2 are currently not conclusively understood.

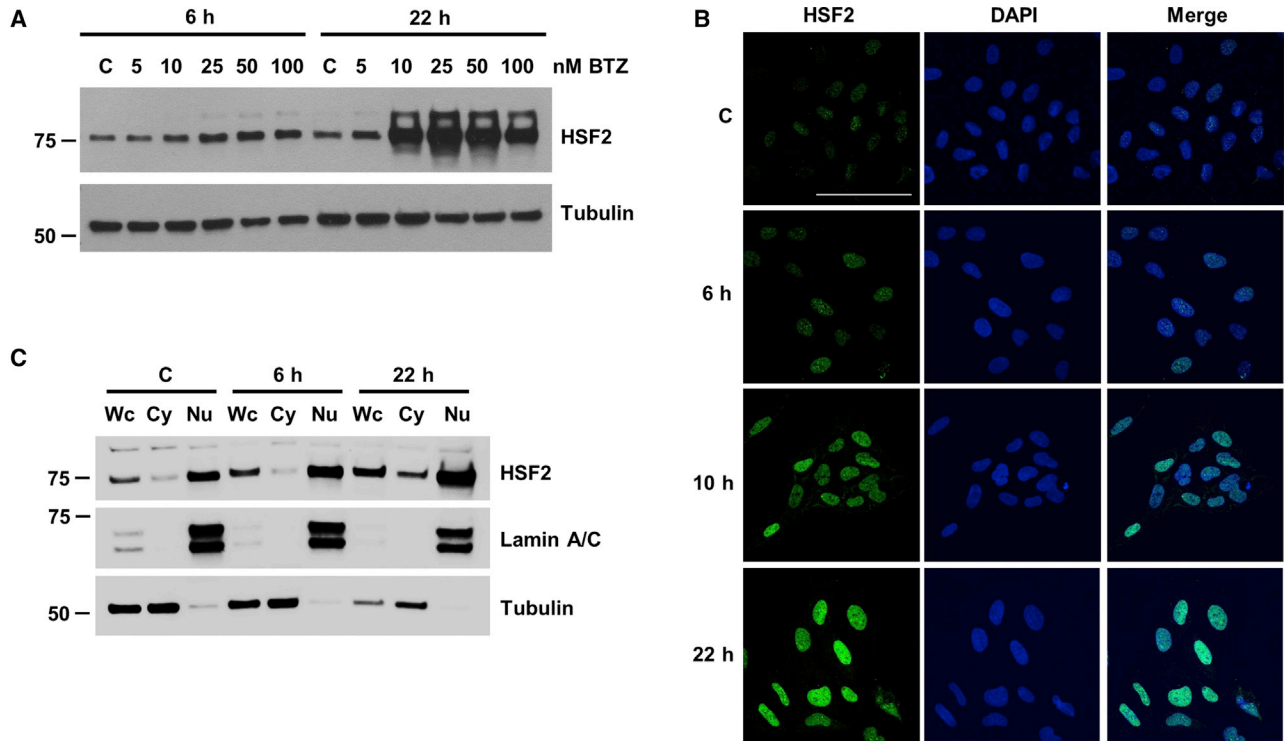

Figure 1. HSF2 Is Upregulated upon Prolonged Bortezomib (BTZ) Treatment

(A) Immunoblot analysis of HSF2 expression. U2OS WT cells were treated with indicated concentrations of BTZ for 6 or 22 h. Control (C) cells were treated with DMSO. Tubulin was used as a loading control.

(B) Confocal microscopy images of HSF2 immunofluorescence staining. U2OS WT cells were plated on coverslips and treated with 25 nM BTZ for 6, 10, or 22 h. Control cells were treated with DMSO. Samples were fixed and stained with anti-HSF2 antibody. DAPI was used for DNA detection. The overlay of HSF2 and DAPI maximum intensity projection signals is shown in merge. Scale bar, 100 μm.

(C) Immunoblot analysis of HSF2 in subcellular fractions. U2OS WT cells were treated with 25 nM BTZ for 6 and 22 h. Control cells were treated with DMSO. Wc, whole cell fraction; Cy, cytoplasmic fraction; and Nu, nuclear fraction. Lamin A/C and Tubulin were used as fractionation controls.

The ubiquitin-proteasome system is one of the main cellular mechanisms regulating protein turnover, thereby affecting multiple aspects of cell physiology, such as signal transduction and apoptosis (Hershko and Ciechanover, 1998; Varshavsky, 2012). Due to the fundamental function in cell physiology, the proteasome complex has emerged as an important target for anti-cancer therapy (Deshaies, 2014). The most common drug to inhibit proteasome function is bortezomib (BTZ; PS-341, VELCADE), which is currently used as a standard treatment in hematological malignancies (Chen et al., 2011). BTZ is a dipeptide boronic acid derivative that targets the chymotrypsin-like activity of the 26S proteasome, causing progressive accumulation of damaged proteins (Kisselev et al., 2006; Chen et al., 2011; Goldberg, 2012). By exposing human blood-derived primary cells to clinically relevant concentrations of BTZ, Rossi and colleagues demonstrated that prolonged proteasome inhibition results in upregulation of HSF2 at both mRNA and protein levels (Rossi et al., 2014). They also showed that HSF2, together with HSF1, localizes to the promoters of *HSP70* and *AIRAP* (zinc finger AN1-type domain 2a) genes (Rossi et al., 2014). In another study, sensitivity to proteasome inhibition was linked to HSF2 deficiency in mouse embryonic fibroblasts (Lecomte et al., 2010), but the mechanisms by which HSF2 promotes cell survival are currently unknown.

In this study, we show that HSF2 is critical for survival of cells during prolonged proteasome inhibition. To our surprise, the genome-wide expression analyses revealed that HSF2 disruption results in a profound downregulation of genes belonging to the cadherin superfamily and subsequent functional impairment of cell-cell adhesion. Furthermore, we show that failure to form adequate cadherin-mediated cell-cell adhesion contacts predisposes cells to proteasome inhibition-induced cell death. These results identify HSF2 as a key regulator of cadherin genes. Taken together, we show that by maintaining cadherin-mediated cell-cell adhesion, HSF2 acts as an important pro-survival factor during sustained proteotoxic stress.

RESULTS

U2OS Cells Lacking HSF2 Are Predisposed to BTZ-Induced Proteotoxicity

To explore the role of HSF2 in prolonged proteotoxic stress, we first examined the expression and cellular localization of HSF2 during BTZ treatment. Human osteosarcoma U2OS cells were treated with different concentrations of BTZ (0–100 nM) for 6 or 22 h and HSF2 protein levels were examined with immunoblotting. The time points were selected to assess both the

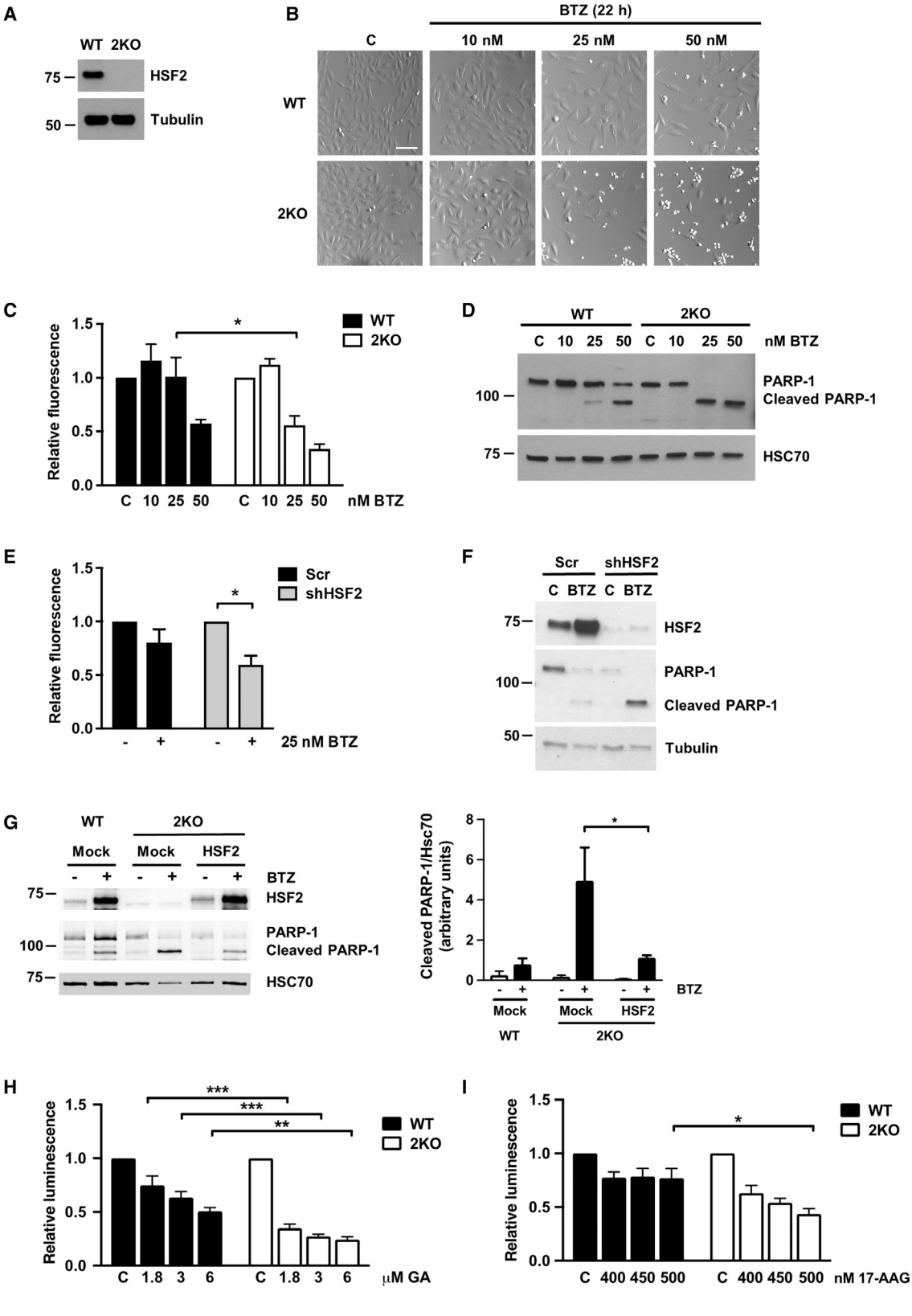

(legend on next page)

short-term and the long-term exposure to BTZ. HSF2 was slightly upregulated already at the 6-h time point and at 22 h its expression was highly elevated (Figure 1A), which is in agreement with a previous report (Rossi et al., 2014). Indirect immunofluorescence and analysis of distinct subcellular fractions revealed that HSF2, which is known to be both cytoplasmic and nuclear (Sheldon and Kingston, 1993; Sistonen et al., 1994), resides predominantly in the nucleus already under control conditions and the nuclear localization is further enhanced during BTZ treatment (Figures 1B and 1C). These results show that cells respond to BTZ treatment with marked increases in HSF2 levels and accumulation in the nucleus.

Next, we asked if HSF2 is required for cell survival under sustained stress conditions. We generated a U2OS *HSF2* knockout cell line (2KO hereafter), where HSF2 expression was abolished by mutating the first exon of the *HSF2* gene using the CRISPR-Cas9 method. In these cells, the protein expression of HSF2 was completely abrogated (Figure 2A). U2OS WT and 2KO cells were treated with indicated concentrations of BTZ for 22 h and examined with microscopy. We observed a dramatic difference in the viability of the wild-type (WT) and 2KO cells, since the cells lacking HSF2 exhibited an apoptotic non-adherent phenotype in concentrations where the WT cells remained adherent (Figure 2B). Quantitative cell viability measurements confirmed that the survival of 2KO cells was significantly impaired upon BTZ treatment (Figure 2C). Furthermore, 2KO cells accumulated more cleaved PARP-1 than WT cells, demonstrating a more pronounced activation of apoptosis (Ling et al., 2002) (Figure 2D). Similar results were obtained with another *HSF2* knockout cell line (2KO#2 hereafter) (Figure S1A) and with *Hsf2*$^{-/-}$ MEFs (mouse embryonic fibroblasts) (Figures S1B and S1C), confirming that the observations are not cell type specific. To verify that the decreased survival of 2KO cells was not caused by off-target effects of the CRISPR-Cas9 gene editing method, we transfected the U2OS WT cells with scramble (Scr) or HSF2-targeting short hairpin RNA (shRNA) plasmids and treated the cells with BTZ for 22 h. In accordance with the results obtained with 2KO cells, transient HSF2 downregulation significantly reduced cell viability upon BTZ treatment and enhanced the progression of apoptosis, which was detected by increased accumulation of cleaved PARP-1 (Figures 2E and 2F). In contrast, re-introduction of HSF2 to the 2KO cells resulted in significantly less cleaved PARP-1 than in the Mock-transfected cells after BTZ treatment (Figure 2G). Hence, we conclude that HSF2 is essential for cell survival upon proteotoxic stress.

In addition to BTZ, treatments with MG132, a well-established proteasome inhibitor, and amino acid analog L-canavanine, which causes protein misfolding when incorporated into nascent peptide chains, clearly reduced the viability of HSF2-deficient cells (Figures S1D–S1H). Importantly, when we exposed the cells to even more extended proteotoxic stress of 46 h, induced by HSP90 inhibitor drugs (Geldanamycin, 17-AAG), the HSF2-deficient cells exhibited reduced survival (Figures 2H and 2I). Altogether these results demonstrate that HSF2 is critical for cell survival upon prolonged accumulation of damaged proteins.

In contrast to HSF2, which has been found to be downregulated in a subset of human cancers (Björk et al., 2016), the expression, nuclear accumulation, and transcriptional activity of HSF1 are increased in a majority of studied cancer types (Björk et al., 2018; Gomez-Pastor et al., 2018). Phosphorylation of serine 326 (pS326) in HSF1 is considered to be a marker for its activation (Guettouche et al., 2005; Mendillo et al., 2012). HSF1 expression and pS326 have been established as requirements for multiple myeloma cell survival during BTZ treatment (Shah et al., 2016). Therefore, we examined whether the decreased survival of 2KO cells was due to impaired HSF1 expression or phosphorylation upon proteasome inhibition. U2OS WT and 2KO cells were treated with BTZ or MG132, and the HSF1 protein levels and S326 phosphorylation status were analyzed with immunoblotting. Importantly, no difference in HSF1 expression or S326 phosphorylation between WT and 2KO cells was observed upon proteasome inhibition (Figure S1I). These results demonstrate that although HSF1 is an essential survival factor during acute stress (Gomez-Pastor et al., 2018), it alone is not sufficient to protect cells against prolonged proteotoxicity.

Figure 2. HSF2 Is Required for Cell Survival upon Prolonged Bortezomib (BTZ) Treatment

(A) Immunoblot analysis of HSF2 expression in U2OS WT and HSF2 KO (2KO) cells. Tubulin was used as a loading control.

(B) Bright-field microscopy images of WT and 2KO cells treated with indicated concentrations of BTZ for 22 h. Control cells were treated with DMSO. Scale bar, 100 μm.

(C) Calcein AM assay of WT and 2KO cells treated as in (B). Relative fluorescence was calculated against each respective control that was set to 1. The data are presented as mean values of at least three independent experiments + SEM; *$p < 0.05$.

(D) Immunoblot analysis of PARP-1. Cells were treated as in (B). HSC70 was used as a loading control.

(E) Calcein AM assay of U2OS WT cells transfected with Scr or HSF2-targeting shRNA constructs (Östling et al., 2007) and treated with 25 nM BTZ for 22 h. Relative fluorescence was calculated against each respective control that was set to 1. The data are presented as mean values of three independent experiments + SEM; *$p < 0.05$.

(F) Immunoblot analysis of HSF2 and PARP-1. Cells were transfected and treated as in (E). Tubulin was used as a loading control.

(G) Immunoblot analysis of HSF2 and PARP-1. HSF2 levels in U2OS 2KO cells were restored to those in WT cells by transiently transfecting the cells with either Mock or HSF2 encoding plasmids. Cells were treated with 25 nM BTZ for 22 h. Control cells were treated with DMSO. HSC70 was used as a loading control. The amount of cleaved PARP-1 relative to HSC70 was quantified with ImageJ. The data are presented as mean values of three independent experiments + SEM; *$p < 0.05$.

(H) CellTiter-Glo assay of U2OS WT and 2KO cells treated with indicated concentrations of Geldanamycin (GA) for 46 h. Control cells were treated with DMSO. Relative luminescence was calculated against each control that was set to 1. The data are presented as mean values of three independent experiments + SEM; **$p < 0.01$ and ***$p < 0.001$.

(I) CellTiter-Glo assay of U2OS WT and 2KO cells treated with indicated concentrations of 17-AAG for 46 h. Control cells were treated with DMSO. Relative luminescence was calculated against each control that was set to 1. The data are presented as mean values of three independent experiments + SEM; *$p < 0.05$.

See also Figure S1.

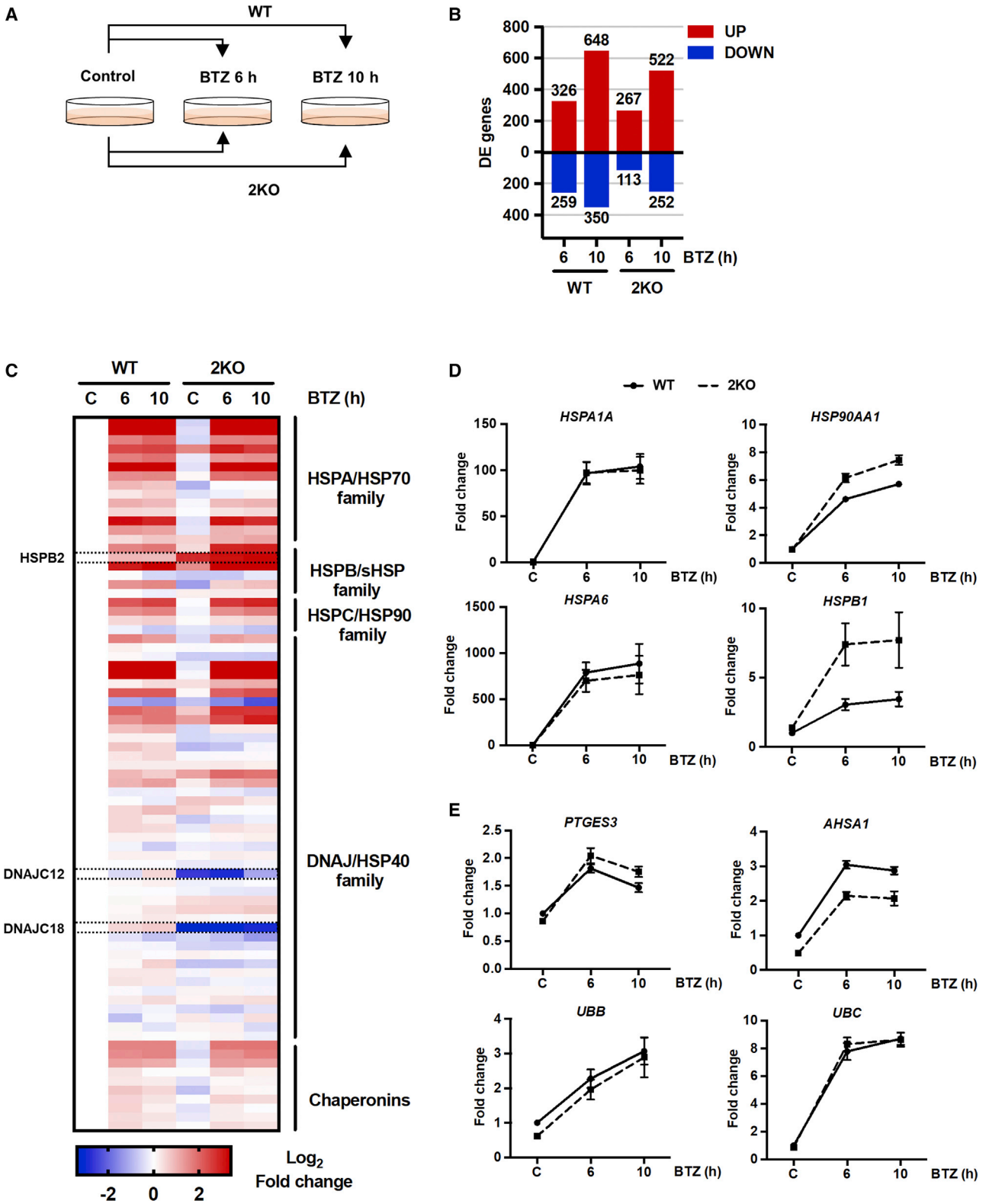

(legend on next page)

Induction of Heat Shock Response Is Not Sufficient to Protect Cells against Proteotoxicity

Similarly to many other surveillance transcription factors, such as p53 (Kubbutat et al., 1997), HIF-1α (Kallio et al., 1999), and Nrf2 (Kobayashi et al., 2004), HSF2 is an unstable protein under normal growth conditions (Ahlskog et al., 2010). HSF2 expression fluctuates in response to stress exposure, tumor progression, and during the cell cycle (Ahlskog et al., 2010: Elsing et al., 2014; Björk et al., 2016), and high expression levels of HSF2 correlate with its increased DNA-binding activity (Mathew et al., 1998; Sarge et al., 1994). Due to the massive increase in nuclear HSF2 levels upon BTZ treatment (Figures 1B and 1C), we investigated if the impaired survival of 2KO cells was caused by misregulation of HSF2 target genes. U2OS WT and 2KO cells were treated with 25 nM BTZ for 6 or 10 h (Figure 3A), and the global gene expression profiles were analyzed with RNA-seq. It is important to note that the selected time points represent sub-lethal proteotoxic stress conditions, at which the cell viability is not yet compromised (Figure S2A). Before mRNA purification, the knockout phenotype was confirmed with immunoblotting (Figure S2B). Stress-inducible hyperphosphorylation of HSF1 (Sarge et al., 1993) and increased HSP70 expression were observed in both WT and 2KO cells (Figure S2B). To identify the HSF2-dependent target genes, we first compared the inducible gene expression profiles between WT and 2KO cells in response to BTZ treatment for 6 and 10 h (Figure 3A). Differentially expressed (DE) genes were determined with the Bioconductor R package Limma (Ritchie et al., 2015), with fold change $\geq$3 and false discovery rate (FDR) <0.001, from quadruplet samples that correlated well to each other (Figure S2C). According to the analysis, BTZ treatment resulted in a significant upregulation and downregulation of genes in WT (>600 and >300, respectively) and 2KO (>500 and >200, respectively) cells (Figure 3B; Table S1). The complete dataset is available at Gene Expression Omnibus under GEO: GSE115973.

The HSF-regulated heat shock response is one of the main cellular survival pathways induced by proteotoxic stress (Joutsen and Sistonen, 2019), and it is characterized by simultaneous upregulation of genes essential for maintaining the correct protein folding environment (Vihervaara et al., 2018). To examine whether the impaired survival of 2KO cells is caused by a compromised heat shock response, we analyzed the inducible expression patterns of all human molecular chaperone genes (Kampinga et al., 2009), in WT and 2KO cells treated with BTZ. Intriguingly, the chaperone expression profiles of WT and 2KO cells were nearly identical, and only *HSPB2*, *DNAJC12*, and *DNAJC18* exhibited distinct expression patterns in 2KO cells (Figure 3C). A closer examination of the RNA-seq data for the expression of selected chaperone genes, i.e., *HSPA1A* (HSP70), *HSP90AA1* (HSP90), *HSPA6* (HSP70B′), and *HSPB1* (HSP27), revealed equal or even higher expression levels in 2KO cells than in WT cells (Figure 3D). In response to proteotoxic stress, HSF2 also localizes to the promoters of genes encoding HSP90 co-chaperones and polyubiquitin (Vihervaara et al., 2013). To study whether the regulation of these genes was disturbed in 2KO cells, HSP90 co-chaperones *PTGES3* (p23) and *AHSA1* (AHA1), as well as the polyubiquitin genes *UBB* and *UBC*, were examined from our RNA-seq data. Since no significant differences were observed in the expression patterns of any of these genes (Figure 3E), we conclude that despite the intact heat shock response, the 2KO cells were not protected against proteotoxic stress. These findings indicate that other determinants, beyond molecular chaperones, govern cell survival during prolonged proteotoxicity.

Disruption of HSF2 Leads to Misregulation of Cell-Adhesion-Associated Genes

To determine the differentially expressed genes between the WT and 2KO cells, we examined the 2KO:WT comparison pair at each experimental time point (0, 6, and 10 h) (Figure 4A). Using the stringent cutoff criteria (fold change [FC] $\geq$ 3; FDR 0.001), 2KO cells were found to display significant misregulation of 819 genes already under normal growth conditions (2KO, C; WT, C), and the proportion of upregulated and downregulated genes remained similar throughout the BTZ treatments (2KO, 6 h; WT, 6 h: 2KO, 10 h; 2KO, 10 h) (Figure 4B; Table S1). Gene Ontology (GO) term analysis of the misregulated genes revealed a specific enrichment of terms related to cell adhesion and cell-cell adhesion via plasma membrane adhesion molecules (Figure 4C; Table S1). Similar GO terms among the comparison pairs implied that the genes misregulated in 2KO cells are tightly linked to cellular adhesion properties both under control and stress conditions (Figure 4C).

To identify the adhesion molecules that are abnormally expressed in 2KO cells under both control and stress conditions, the gene set overlaps were examined with Venn diagrams. Among the comparison pairs, a total of 114 and 277 genes were upregulated and downregulated, respectively (Figure 4D). Functional cluster annotation of the 114 upregulated genes with the DAVID analysis tool (Dennis et al., 2003) confirmed

Figure 3. Induction of the Heat Shock Response Is Not Sufficient to Protect HSF2-Deficient Cells against BTZ-Induced Proteotoxic Stress

(A) A schematic overview of the RNA-seq experiment outline. U2OS WT and 2KO cells were treated with 25 nM BTZ for 6 or 10 h. Control cells were treated with DMSO. After treatments, mRNA was extracted and analyzed by RNA-seq. Experiments were performed in biological quadruplets. The arrows depict comparison pairs.

(B) Differentially expressed (DE) genes in each comparison pair were determined with the Bioconductor R package Limma (Ritchie et al., 2015) (FC $\geq$ 3; FDR < 0.001). The upregulated and downregulated genes in a given comparison pair are indicated with red and blue bars, respectively.

(C) Normalized gene expression data for human heat shock proteins, as defined in Kampinga et al. (2009), was used to calculate the fold change of each gene in relation WT control sample. The data are presented as a heatmap of $\log_2$-transformed values and were generated with GraphPad Prism7. Examples of genes that exhibit a divergent expression pattern are framed.

(D and E) mRNA expression levels of selected heat shock proteins (*HSPA1A*, *HSP90AA1*, *HSPA6*, and *HSPB1)* (D), HSP90 co-chaperones (*PTGES3* and *AHSA1*), and stress-responsive ubiquitin genes (*UBB* and *UBC*) (E) determined with RNA-seq. The data are presented as mean values ± SEM relative to WT control sample that was set to 1.

See also Figure S2 and Table S1.

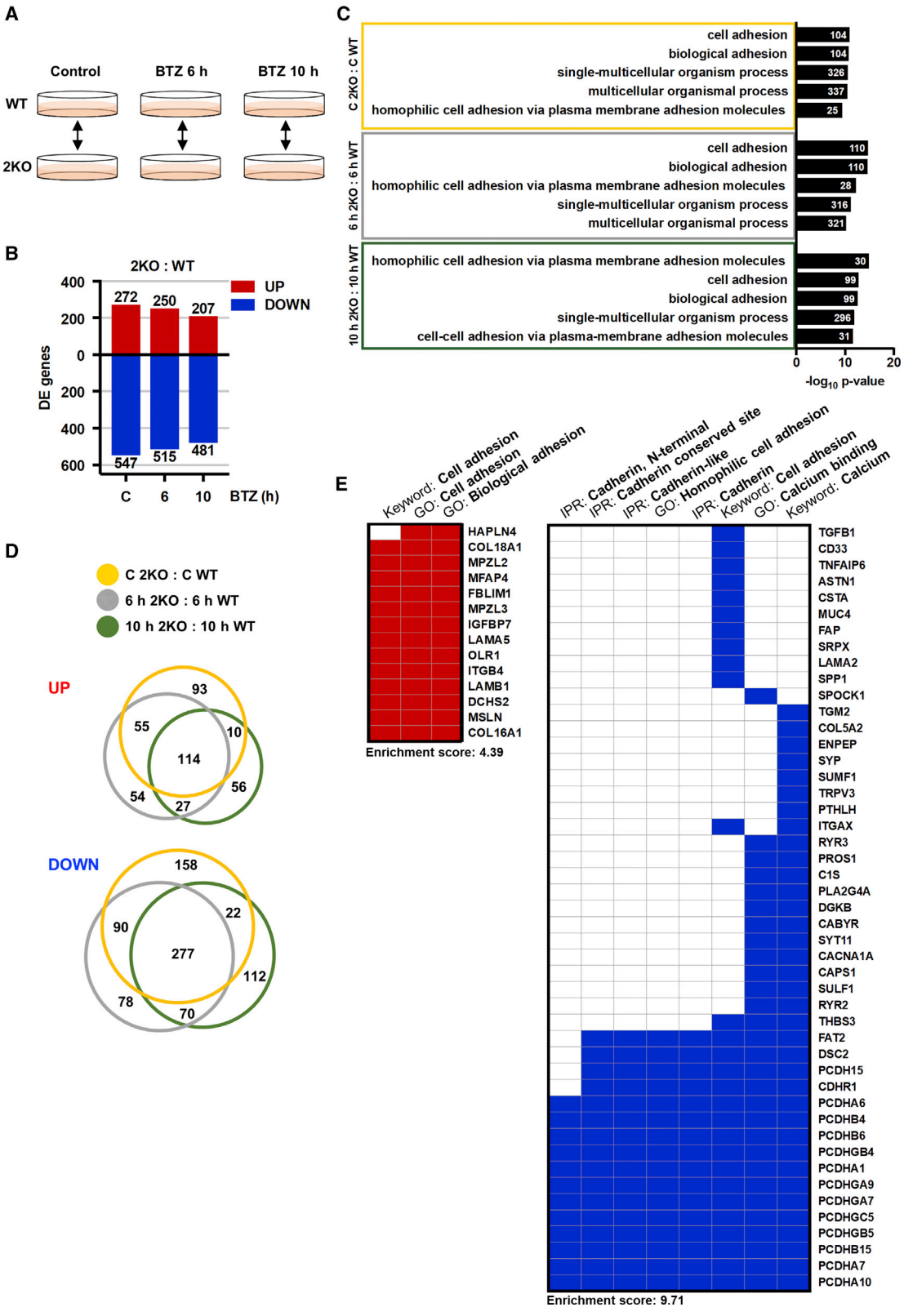

(legend on next page)

the strong association to cell adhesion and an extracellular matrix, including collagens (*COL16A1* and *COL18A1*) and laminins (*LAMB1* and *LAMA5*) (Figure 4E, left panel; Figure S3). Interestingly, the 277 downregulated genes included members from multiple cadherin sub-families, such as protocadherins (*PCDHA1* and *PCDHA7*), desmosomal cadherins (*DSC2*), and Fat-Dachsous cadherins (*FAT2*), suggesting that the cadherin-mediated cell adhesion was extensively misregulated in 2KO cells (Figure 4E, right panel). The most prominent changes were detected in protocadherins, as 13 distinct protocadherin genes were significantly downregulated in 2KO cells both under normal growth conditions and upon exposure to BTZ-induced stress (Figure 4E).

Cells Lacking HSF2 Display Abnormal Cadherin Expression

Cadherins are transmembrane adhesion molecules that mediate Ca^{2+}-dependent cell-cell adhesion via the conserved extracellular cadherin domains (Hirano and Takeichi, 2012). The human genome encodes 110 cadherin genes, which together form the cadherin superfamily consisting of distinct cadherin sub-families (Hirano and Takeichi, 2012). Since the cadherin genes appeared as an HSF2-dependent gene group and showed significant misregulation in multiple sub-family members, we examined the expression profiles of all cadherin superfamily genes in 2KO cells. Normalized gene expression data were used to generate a heatmap encompassing all cadherin genes encoded by the human genome. By comparing the expression profiles of WT and 2KO cells in control and BTZ-induced stress conditions, we observed a prominent downregulation of the entire cadherin superfamily. At least one member from every sub-family was found downregulated in 2KO cells, including classical cadherins (*CDH2* and *CDH6*), desmosomal cadherins (*DSC2* and *DSG2*), CDH23-PCDH15 cadherins (*CDH12*), Fat-Dachsous cadherins (*FAT2* and *FAT4*), Flamingo cadherins (*CELSR1*), and Calsyntenins (*CLSTN2*) (Figure 5A; Table S1). The most striking downregulation was detected in clustered α-, β-, and γ-protocadherins (Peek et al., 2017), of which a majority were found to be abnormally expressed in 2KO cells (Figure 5A). Based on these results, we propose that cadherins are the main adhesion molecules downregulated in HSF2-depleted U2OS cells.

For understanding the biological relevance of the RNA-seq analyses, we determined the protein expression levels of classical cadherins (Pan-Cadherin), N-cadherin (*CDH2*), and clustered γ-protocadherins (Pan-PCDHγA) by immunoblotting. As shown in Figure 5B, classical cadherins, specifically N-cadherin, and γ-protocadherins were significantly downregulated also at the protein level (Figure 5B), and the downregulation was maintained throughout the BTZ treatment (Figure S4A). Since cadherins are essential in mediating Ca^{2+}-dependent cell-cell contacts, we examined the functional impact of our observations using a cell aggregation assay, where single cells were allowed to freely make cell-cell adhesion contacts in suspension. U2OS WT and 2KO cells were suspended in cell aggregation buffer supplemented with either $CaCl_2$ or EDTA. WT cells supplemented with Ca^{2+} formed large cell aggregates, which were completely abolished in Ca^{2+}-chelating conditions (EDTA) (Figures 5C and S4B). In stark contrast, 2KO cells were unable to form cell aggregates even in the presence of Ca^{2+} (Figures 5C and S4B), indicating that HSF2 is required to maintain cadherin-mediated cell-cell contacts.

Loss of distinct cell-cell adhesion molecules has been associated with cellular inability to form three-dimensional (3D) spheroids in ultra-low attachment (ULA) round bottom plates (Stadler et al., 2018). When U2OS WT and 2KO cells were grown on ULA plates, we found that WT cells formed compact spheroids in 48 h. In contrast, 2KO cells were not able to integrate into compact spheres, thereby occupying a significantly larger area of the ULA plates (Figure 5D). Similar spheroid-forming phenotypes were observed when WT and 2KO cells were grown on bacterial plates (Figure S4C). We further explored the spheroid-forming capacity by culturing the cells in a 3D extracellular matrix (ECM) and the *in vivo* tumor growth with chicken chorioallantoic membrane (CAM) assay. As expected, the spheroids and tumors originating from 2KO cells were significantly smaller than the WT counterparts (Figures 5E and S4D), further strengthening the findings of functional impairment of cell-cell adhesion in the absence of HSF2. A profound decline in the expression and function of cadherin superfamily proteins was also observed in 2KO#2 cells (Figures S4E–S4H), demonstrating that the alterations are not specific for a single-cell clone. Altogether these results show that the lack of HSF2 leads to disrupted cadherin expression at the mRNA and protein levels, thereby resulting in deterioration of cadherin-mediated cell-cell adhesion.

Impaired Cell-Cell Adhesion Sensitizes Cells to Proteotoxic Stress

Although it is well acknowledged that cadherins are essential mediators of tissue integrity and pivotal in regulating the development of multicellular organisms (Hirano and Takeichi, 2012; Peek et al., 2017), their impact on proteotoxic stress resistance

Figure 4. HSF2 Regulates Expression of Genes Associated with Cadherin-Mediated Cell-Cell Adhesion

(A) A schematic overview of the U2OS WT and 2KO comparison pairs.

(B) DE genes in 2KO:WT comparison pairs (control, 6 h, and 10 h) were determined with the Bioconductor R package Limma (Ritchie et al., 2015) (FC ≥ 3; FDR < 0.001). The upregulated and downregulated genes are indicated with red and blue bars, respectively.

(C) Gene Ontology (GO) terms were analyzed with topGO and GOstats packages in Bioconductor R. Biological processes from each comparison pair were ranked according to their p values and the five most significantly changed GO terms are shown. The number of genes associated with a given term is indicated.

(D) Venn diagrams presenting the interrelationship of significantly (FC ≥ 3; FDR < 0.001) upregulated or downregulated genes in 2KO:WT comparison pairs at control (orange), 6-h (gray), and 10-h (green) time points. Diagrams were generated using the BioVenn web application.

(E) Gene term heatmap generated with DAVID Functional Annotation Clustering Tool based on the 114 upregulated (left panel) and the 277 downregulated (right panel) genes in 2KO cells in all treatment conditions as shown in (D). Red and blue squares denote positive association between the gene and the keyword, GO term, or InterPro (IPR) term. Cluster enrichment score for the upregulated gene cluster is 4.39 and for the downregulated gene cluster it is 9.71.

See also Figure S3 and Table S1.

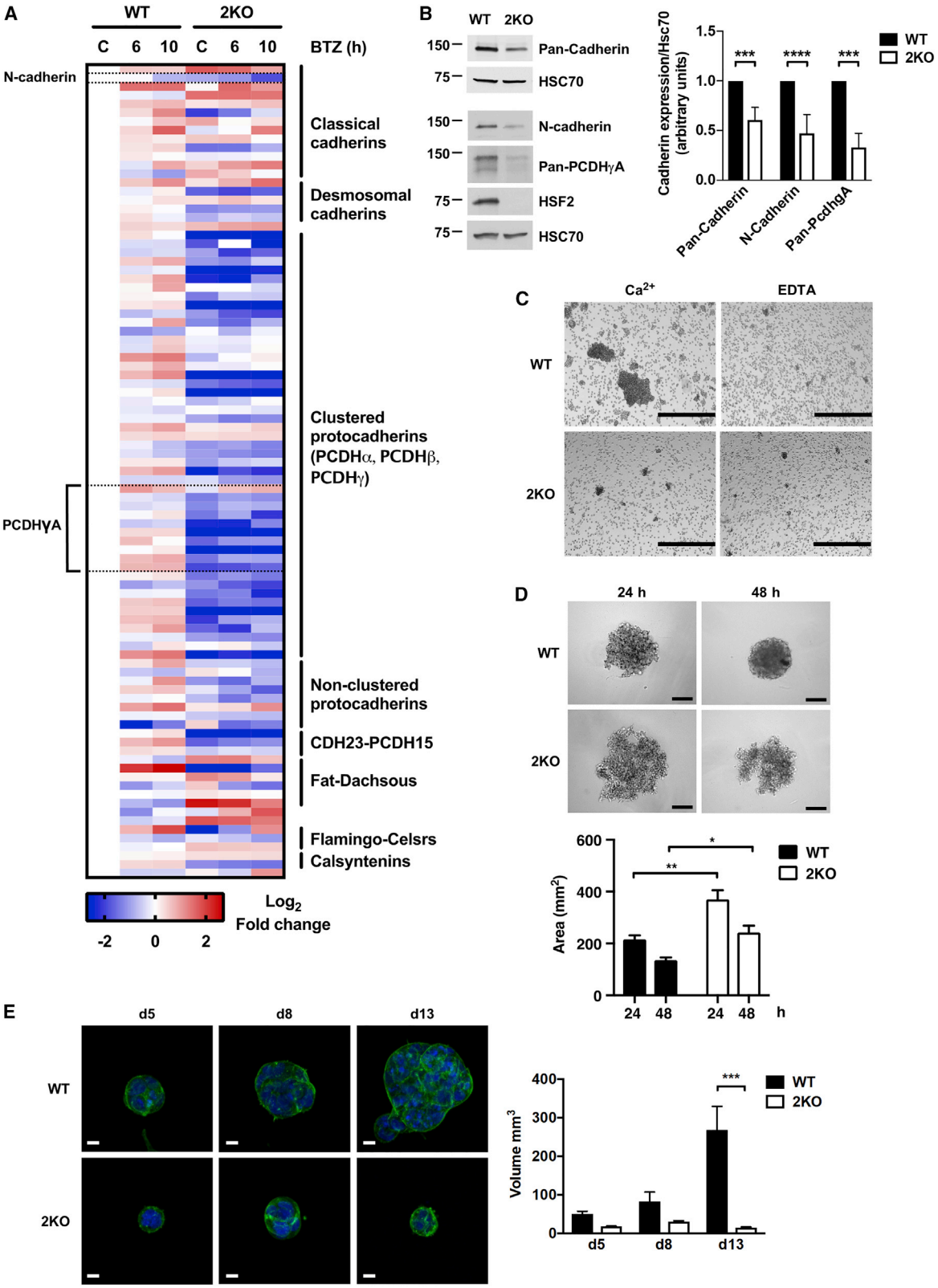

(legend on next page)

has remained unexplored. To examine whether the observed impairment of cell-cell adhesion in 2KO cells also contributes to the susceptibility of the cells to BTZ-induced stress, we restored the cellular adhesion properties by re-introducing N-cadherin to 2KO cells. N-cadherin was selected for these experiments, because it is the most abundantly expressed cadherin superfamily member in WT U2OS cells, according to our RNA-seq data (GEO: GSE115973), and it was found to be downregulated in 2KO cells. WT and 2KO cells were transfected with either Mock or N-cadherin plasmids, and the N-cadherin expression was examined with immunoblotting (Figure 6A). As shown in Figure 6A, we were able to restore the N-cadherin levels in 2KO cells, which resulted in a functional rescue of cell-cell adhesion in 2KO cells (Figure 6B). Importantly, when exposed to BTZ, the 2KO cells expressing exogenous N-cadherin displayed significantly less cleaved PARP-1 than the Mock-transfected cells (Figures 6C, 6D, and S5), suggesting that restoration of cell-cell adhesion can suppress cell death caused by BTZ-induced proteotoxic stress.

All cadherin superfamily proteins are characterized by extracellular cadherin repeat domains, which mediate homophilic adhesion contacts between adjacent cells (Seong et al., 2015). Stabilization of the extracellular domains is regulated by Ca^{2+}, which binds to the interdomain regions of the consecutive cadherin repeats and rigidifies the ectodomain structure. To be able to comprehensively investigate the role of cadherins in the cellular resistance to proteotoxic stress, we first treated WT U2OS cells and MEFs with BTZ for 20 h to induce proteotoxic stress, after which the whole cadherin-mediated cell-cell adhesion program was destabilized by specifically depleting the extracellular Ca^{2+} with EGTA (Figure 6E). Serum-free culture conditions were used for complete depletion of extracellular Ca^{2+}. We observed that Ca^{2+} depletion intensified cell death, which was evidenced by the enhanced PARP-1 and Caspase-3 cleavage in WT U2OS cells and MEFs, respectively, after a combined treatment with both BTZ and EGTA (Figure 6F). Altogether, these results show that cadherin-mediated cell-cell adhesion is a key determinant of cell survival upon BTZ treatment and that destabilization of cadherin contacts predisposes cells to stress-induced proteotoxicity.

DISCUSSION

Maintenance of cellular proteostasis is fundamental for the viability of all cells and organisms (Joutsen and Sistonen, 2019). The heat shock response is critical for promoting proteostasis and it is under strict control of the HSFs, among which HSF1 is considered as the main factor responding to acute stress. Until now, the role of HSF2 in the cellular response to sustained proteotoxicity has remained unknown. We hypothesized that HSF2 is required to protect cells against progressive accumulation of protein damage. To test this hypothesis, we used proteasome inhibitors (BTZ and MG132), L-Canavanine, and HSP90 inhibitors as our experimental tools to induce long-term proteotoxic stress. BTZ treatment has been previously shown to upregulate HSF2 at both mRNA and protein levels in blood-derived human primary cells and to induce HSF2 binding at designated gene loci (Rossi et al., 2014). Our data showed that BTZ treatment also leads to a remarkable increase in HSF2 protein levels in malignant human cells. Moreover, we demonstrate that the amount of nuclear HSF2 is markedly increased in BTZ-treated cells, showing that HSF2 specifically responds to proteasome inhibition. We found that HSF2 is not only activated by BTZ-induced proteotoxicity, but it is absolutely essential for cell survival under these conditions. Based on our results, we conclude that HSF2 is required to protect cells against progressive accumulation of damaged proteins.

Elevated protein levels of HSF1 and its phosphorylation on serine 326 were recently shown to be a prerequisite for multiple myeloma cell survival upon BTZ treatment (Shah et al., 2016; Fok et al., 2018). Therefore, we explored whether HSF2 depletion sensitizes cells to BTZ through misregulated HSF1, specifically, or the heat shock response in general. Neither difference in HSF1 levels nor serine 326 phosphorylation was detected between WT and HSF2-depleted cells treated with proteasome inhibitors. Strikingly, the classical heat shock response, as characterized by the global upregulation of molecular chaperones, HSP90 co-chaperones, and polyubiquitin genes, was not compromised in cells lacking HSF2. These results indicate that HSF2 promotes cell survival independently of HSF1. Thus, we provide evidence that the ability to survive proteotoxic stress does not solely

Figure 5. HSF2 Controls Cellular Adhesion Properties through Cadherin Superfamily Proteins

(A) Normalized gene expression data from the RNA-seq analysis for cadherin superfamily genes, as defined in Hirano and Takeichi (2012), was used to calculate the fold change of each gene in relation to respective expression in the WT control sample. The data are presented as a heatmap of log_2-transformed fold changes and were generated with GraphPad Prism7. N-cadherin and protocadherin gamma subfamily A (PCDHγA) were chosen for further analyses.

(B) Immunoblot analysis of classical cadherins, N-cadherin, and the members of PCDHγA in U2OS WT and 2KO cells. Lack of HSF2 expression in 2KO cells was confirmed and HSC70 was used as a loading control. The amount of cadherins relative to respective HSC70 level was quantified with ImageJ. The data are presented as mean values of three independent experiments + SEM; ***$p < 0.001$ and ****$p < 0.0001$.

(C) Cell aggregation assay of U2OS WT and 2KO cells suspended in cell aggregation buffer supplemented with 3 mM $CaCl_2$ (Ca^{2+}) or 3 mM EDTA. Cells were rotated for 2.5 h at 37°C and visualized with bright-field microscopy. Scale bar, 1 mm.

(D) Bright-field microscopy images of U2OS WT and 2KO cells cultured in ULA plates. Cells were imaged after 24 and 48 h. Scale bar, 200 μm. The size of the spheroid area was quantified with ImageJ. The data are presented as mean values of three independent experiments + SEM. *$p < 0.05$ and **$p < 0.01$.

(E) Confocal microscopy images of U2OS WT and 2KO cells. Cells were cultured in 3D in Matrigel for 5, 8, and 13 days. At the indicated days, spheroids were fixed, and F-actin was stained with Alexa 488-labeled phalloidin (green). DAPI was used to stain the nuclei (blue). *Z* stacks of the spheroids were imaged with a spinning disc confocal microscope. The maximum intensity projection images represent the average spheroid size for each cell line at indicated time points from three biological repeats. Scale bar, 10 μm. The volume of the spheroids was quantified with ImageJ with the 3D Object Counter v2.0 plugin (Bolte and Cordelières, 2006). The data are presented as mean values of three independent experiments + SEM. ***$p < 0.001$.

See also Figure S4.

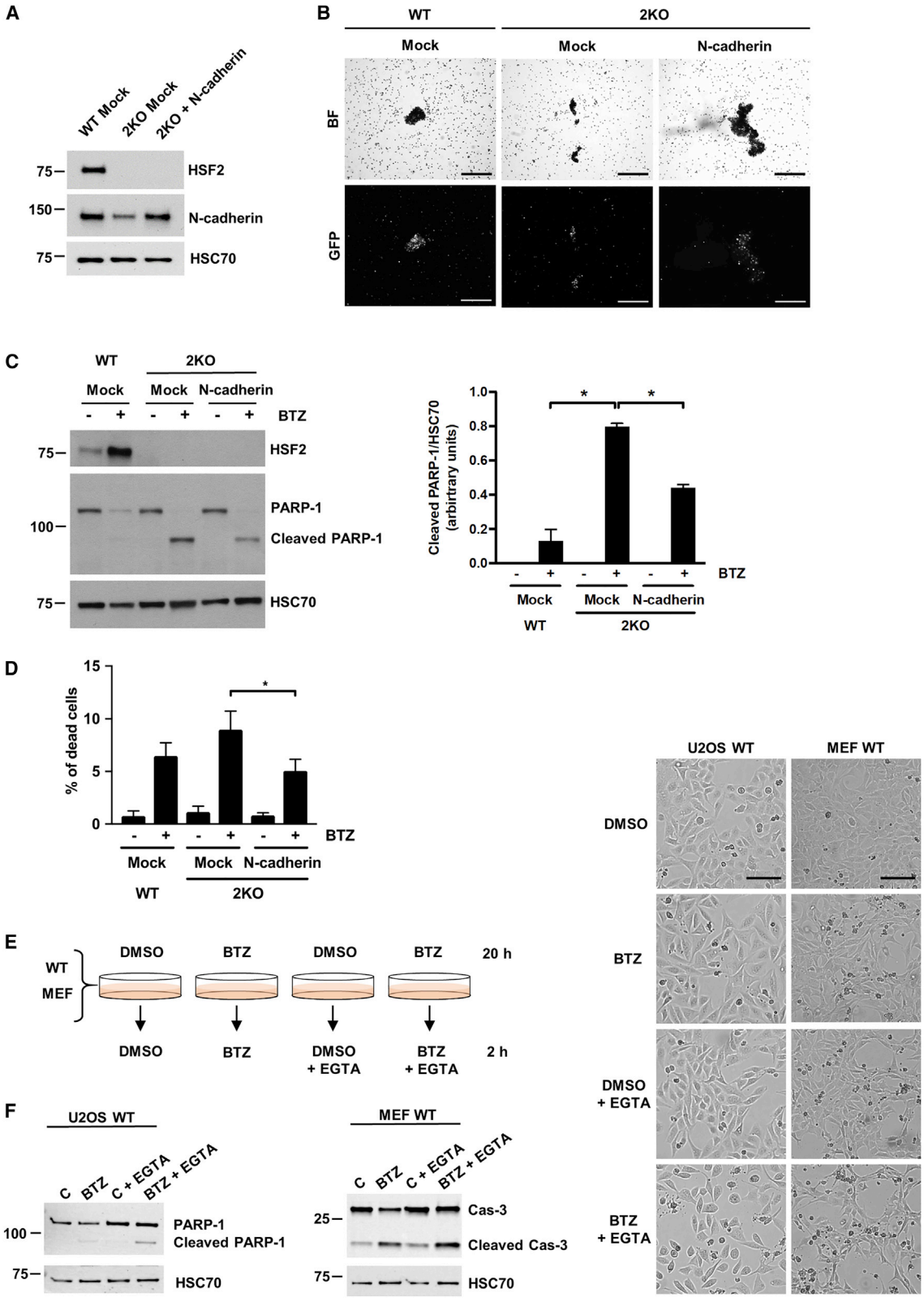

(legend on next page)

depend on the induction of molecular chaperones but engages a larger repertoire of cellular pathways and properties.

To our surprise, despite the stringent cutoff criteria (FC $\geq$ 3; FDR 0.001), we found a considerable number of genes displaying altered expression profiles in cells lacking HSF2. Among the most prominently misregulated genes were those belonging to the cadherin superfamily. Here, we demonstrate that lack of HSF2 leads to a profound downregulation of cadherins both at mRNA and protein levels, identifying HSF2 as a key regulator of cadherin genes. Cadherins are a large group of transmembrane adhesion molecules, which mediate Ca^{2+}-dependent cell-cell adhesion and thereby function as essential mediators of tissue integrity (Hirano and Takeichi, 2012). We found that HSF2-deficient cells display functional impairment of cadherin-mediated cell-cell adhesion already under normal growth conditions. Together with earlier results of HSF2 displaying DNA-binding capacity already in the absence of stress (Sarge et al., 1991; Åkerfelt et al., 2008; Vihervaara et al., 2013), these results suggest that HSF2 has a physiological role in regulating cadherin functions. Excitingly, impaired migration and mispositioning of neurons have been shown to underlie the corticogenesis defects in *Hsf2*$^{-/-}$ mice (Kallio et al., 2002; Chang et al., 2006), and cadherin superfamily proteins are fundamental for correct neuronal migration (Hayashi and Takeichi, 2015). Thus, it is tempting to speculate that the HSF2-dependent disruption of cadherin-mediated cell-cell contacts contributes to the abnormal corticogenesis of *Hsf2*$^{-/-}$ mice.

The downregulation of cadherin gene expression raises important questions about the mechanisms by which HSF2 regulates these genes. Genome-wide mapping of HSF2 binding sites has been previously determined with chromatin immunoprecipitation sequencing (ChIP-seq) in human K562 erythroleukemia cells (Vihervaara et al., 2013) and in mouse testis (Korfanty et al., 2014). Remarkably, both studies identified HSF2 occupancy on multiple cadherin superfamily genes. Since non-adherent K562 cells are deficient of endogenously expressed classical cadherins and distinct protocadherins (Ozawa and Kemler, 1998), it is not surprising that HSF2 was found to occupy only the *CLSTN* gene under control growth conditions (Vihervaara et al., 2013). However, upon acute heat stress, HSF2 binding was observed at classical cadherins (*CDH4*), desmogleins (*DSG2*), Fat-Dachous cadherins (*DCHS2*), Flamingo cadherins (*CELSR2*), and CDH23-PCDH15 cadherins (*CDH23*) (Vihervaara et al., 2013), demonstrating that multiple genes belonging to the cadherin superfamily can be targeted by HSF2 in human cells. In mouse testis, HSF2 was also shown to occupy several cadherin genes, including *CDH15*, *CDH5*, *CDH18*, *CDH13*, *FAT1*, *PCDH9*, *PCDH17*, and *PCDHA1* (Korfanty et al., 2014). Importantly, we now demonstrate the functional relevance of HSF2-mediated cadherin regulation and propose HSF2 as a central regulator of cadherin genes.

Failure in the maintenance of proteostasis is a hallmark of aging and neurodegenerative diseases (Douglas and Dillin, 2010). Intriguingly, in a mouse model of Huntington's disease, lack of HSF2 was shown to predispose mouse brain to poly-Q aggregates and reduce lifespan (Shinkawa et al., 2011), suggesting that HSF2 is required to protect neurons from progressive accumulation of damaged proteins. Cell survival upon proteotoxic stress has been conventionally considered to depend on inducible transcriptional programs, such as the heat shock response or the unfolded protein response (Walter and Ron, 2011; Gomez-Pastor et al., 2018). However, in this study, we show that HSF2-dependent maintenance of cell-cell adhesion is an essential determinant of proteotoxic stress resistance. Our results indicate that misregulation of distinct cellular properties already under normal growth conditions can sensitize cells to proteotoxicity. HSF1 and HSF2 represent the two arms of the cellular resistance toward proteotoxic stress; HSF1 as an acute responder to protein damage and HSF2 as a factor maintaining the long-term stress resistance. Notably, in a meta-analysis of transcriptional changes associated with Alzheimer's disease and aging, HSF2 was identified as a gene commonly downregulated during aging (Ciryam et al., 2016). Therefore, it is possible that the age-associated downregulation of HSF2 and subsequent disruption of cadherin-mediated cell-cell adhesion participates in sensitizing cells, such as neurons, to aggregate mismanagement.

STAR★METHODS

Detailed methods are provided in the online version of this paper and include the following:

- KEY RESOURCES TABLE
- LEAD CONTACT AND MATERIALS AVAILABILITY

Figure 6. Impaired Cell-Cell Contacts Sensitize Cells to BTZ-Induced Proteotoxic Stress

(A–D) N-cadherin levels in U2OS 2KO cells were restored to those in WT cells by transiently transfecting the cells with either Mock or N-cadherin plasmids co-expressing GFP.

(A) Immunoblot analysis of HSF2 and N-cadherin. HSC70 was used as a loading control.

(B) Cell aggregation assay was performed as in Figure 5C. Cell aggregates were imaged with bright-field (BF) and fluorescence filters (GFP). Scale bar, 500 μm.

(C) For immunoblot analysis of HSF2 and PARP-1, cells were treated with 25 nM BTZ for 22 h. Control cells were treated with DMSO. HSC70 was used as a loading control. The amount of cleaved PARP-1 relative to the respective HSC70 level was quantified with ImageJ. The data are presented as mean values of three independent experiments + SEM; *$p < 0.05$.

(D) Flow cytometry analysis of fluorescently labeled cleaved PARP-1 antibody. Cells were treated with 25 nM BTZ for 22 h. Control cells were treated with DMSO. The data are presented as mean values of three independent experiments + SEM; *$p < 0.05$. The statistical analysis was performed with a Student's t test.

(E) A schematic overview of the calcium-depletion experiments.

(F) U2OS WT cells were treated with or without 25 nM BTZ for 20 h in serum-free growth medium after which the extracellular calcium was depleted with 4 mM EGTA and BTZ treatment continued for 2 h. MEFs were treated with 5 or 10 nM BTZ for 20 h in serum-free growth medium after which the extracellular calcium was depleted with 2 mM EGTA and BTZ continued for 2 h. Control cells were treated with DMSO. PARP-1 and Caspase-3 cleavage was assessed with immunoblotting. Cells were imaged with a bright-field microscope. Scale bar, 200 μm.

See also Figure S5.

SUPPLEMENTAL INFORMATION

Supplemental Information can be found online at https://doi.org/10.1016/j.celrep.2019.12.037.

ACKNOWLEDGMENTS

We thank Joshua Weiner (University of Iowa, Iowa, US) for helpful discussions and advice and for providing us with the anti-PanPCDHγA antibody. Mikael Puustinen from the Sistonen laboratory is acknowledged for his assistance with the CAM-assay. All members of the Sistonen laboratory and Véronique Dubreuil from the Mezger laboratory are thanked for their valuable comments and critical review of the manuscript. Imaging was performed at the Cell Imaging Core, Turku Bioscience Centre, University of Turku and Åbo Akademi University. The instruments used in this project belong to the infrastructure of Biocenter Finland. We thank Markku Saari and Jouko Sandholm from the Cell Imaging Core of Turku Bioscience Centre for technical assistance and advice. The Bioinformatics unit of Turku Bioscience Centre is acknowledged for their assistance with the RNA-seq data analysis. The Bioinformatics unit is supported by University of Turku, Åbo Akademi University, and Biocenter Finland. This study has been funded by the Academy of Finland (L.S.); Sigrid Juselius Foundation (L.S.); Turku Doctoral Network in Molecular Biosciences (A.J.D.S. and J.C.L.); Finnish Cultural Foundation (J.J.); Cancer Foundation Finland (J.J. and L.S.); Åbo Akademi University Research Foundation (J.J. and M.A.B.); Magnus Ehrnrooth Foundation (A.J.D.S. and L.S.); Tor, Joe and Pentti Borg Memory Foundation (J.J.); Ida Montin's Foundation (J.J.); Otto A. Malm Foundation (J.J. and A.J.D.S.); the Medical Research Foundation Liv och Hälsa (J.J. and L.S.); K. Albin Johansson's Foundation (J.J., A.J.D.S., and E.H.); Agence Nationale Recherche (Program SAMENTA ANR-13-SAMA-0008-01; A.d.T., V.M., and D.S.-D.); Short Researcher Mobility France Embassy/MESRI-Finnish Society of Science and Letters (V.M.); and CNRS/Project International de Coopération Scientifique PICS 2013-2015 (A.d.T., V.M., and D.S.-D.).

AUTHOR CONTRIBUTIONS

J.J., A.J.D.S., and L.S. designed the research; J.J., A.J.D.S., J.C.L., M.A.B., A.S.N., and E.H. performed the experiments; A.d.T., J.-P.C., V.M., and D.S.-D. generated and analyzed the U2OS cell lines; J.J., A.J.D.S., J.C.L., E.H., and L.S. analyzed the data; and J.J., A.J.D.S., and L.S. wrote the manuscript with all authors providing feedback.

DECLARATION OF INTERESTS

The authors declare no competing interests.

Received: June 19, 2019
Revised: October 15, 2019
Accepted: December 12, 2019
Published: January 14, 2020

REFERENCES

Ahlskog, J.K., Björk, J.K., Elsing, A.N., Aspelin, C., Kallio, M., Roos-Mattjus, P., and Sistonen, L. (2010). Anaphase-promoting complex/cyclosome participates in the acute response to protein-damaging stress. Mol. Cell. Biol. *30*, 5608–5620.

Åkerfelt, M., Henriksson, E., Laiho, A., Vihervaara, A., Rautoma, K., Kotaja, N., and Sistonen, L. (2008). Promoter ChIP-chip analysis in mouse testis reveals Y chromosome occupancy by HSF2. Proc. Natl. Acad. Sci. USA *105*, 11224–11229.

Åkerfelt, M., Morimoto, R.I., and Sistonen, L. (2010). Heat shock factors: integrators of cell stress, development and lifespan. Nat. Rev. Mol. Cell Biol. *11*, 545–555.

Alastalo, T.P., Lönnström, M., Leppä, S., Kaarniranta, K., Pelto-Huikko, M., Sistonen, L., and Parvinen, M. (1998). Stage-specific expression and cellular localization of the heat shock factor 2 isoforms in the rat seminiferous epithelium. Exp. Cell Res. *240*, 16–27.

Alexa, A., and Rahnenfuhrer, J. (2019). topGO: Enrichment Analysis for Gene Ontology. R package version 2.37.0. https://bioconductor.org (Bioconductor).

Andrews, S. (2010). FastQC: a quality control tool for high throughput sequence data. Babraham Bioinformatics. www.bioinformatics.babraham.ac.uk/projects/fastqc.

Björk, J.K., Ahonen, I., Mirtti, T., Erickson, A., Rannikko, A., Bützow, A., Nordling, S., Lundin, J., Lundin, M., Sistonen, L., Nees, M., and Åkerfelt, M. (2018). Increased HSF1 expression predicts shorter disease-specific survival of prostate cancer patients following radical prostatectomy. Oncotarget *9*, 31200–31213.

Björk, J.K., Åkerfelt, M., Joutsen, J., Puustinen, M.C., Cheng, F., Sistonen, L., and Nees, M. (2016). Heat-shock factor 2 is a suppressor of prostate cancer invasion. Oncogene *35*, 1770–1784.

Bolte, S., and Cordelières, F.P. (2006). A guided tour into subcellular colocalization analysis in light microscopy. J. Microsc. *224*, 213–232.

Budzyński, M., and Sistonen, L. (2017). Versatile Functions of Heat Shock Factors: It Is Not All about Stress. Curr. Immunol. Rev. *13*, 4–18.

Chang, Y., Östling, P., Åkerfelt, M., Trouillet, D., Rallu, M., Gitton, Y., El Fatimy, R., Fardeau, V., Le Crom, S., Morange, M., et al. (2006). Role of heat-shock factor 2 in cerebral cortex formation and as a regulator of p35 expression. Genes Dev. *20*, 836–847.

Chen, D., Frezza, M., Schmitt, S., Kanwar, J., and Dou, Q.P. (2011). Bortezomib as the first proteasome inhibitor anticancer drug: current status and future perspectives. Curr. Cancer Drug Targets *11*, 239–253.

Ciryam, P., Kundra, R., Freer, R., Morimoto, R.I., and Dobson, C.M. (2016). A transcriptional signature of Alzheimer's disease is associated with a metastable subproteome at risk for aggregation. Proc. Natl. Acad. Sci. USA *113*, 4753–4758.

Dennis, G., Jr., Sherman, B.T., Hosack, D.A., Yang, J., Gao, W., Lane, H.C., and Lempicki, R.A. (2003). DAVID: Database for Annotation, Visualization, and Integrated Discovery. Genome Biol. *4*, 3.

Deshaies, R.J. (2014). Proteotoxic crisis, the ubiquitin-proteasome system, and cancer therapy. BMC Biol. *12*, 94.

Douglas, P.M., and Dillin, A. (2010). Protein homeostasis and aging in neurodegeneration. J. Cell Biol. *190*, 719–729.

Elsing, A.N., Aspelin, C., Björk, J.K., Bergman, H.A., Himanen, S.V., Kallio, M.J., Roos-Mattjus, P., and Sistonen, L. (2014). Expression of HSF2 decreases in mitosis to enable stress-inducible transcription and cell survival. J. Cell Biol. *206*, 735–749.

Falcon, S., and Gentleman, R. (2007). Using GOstats to test gene lists for GO term association. Bioinformatics *23*, 257–258.

Fok, J.H.L., Hedayat, S., Zhang, L., Aronson, L.I., Mirabella, F., Pawlyn, C., Bright, M.D., Wardell, C.P., Keats, J.J., De Billy, E., et al. (2018). HSF1 Is essential for myeloma cell survival and a promising therapeutic target. Clin. Cancer Res. *24*, 2395–2407.

Gentleman, R.C., Carey, V.J., Bates, D.M., Bolstad, B., Dettling, M., Dudoit, S., Ellis, B., Gautier, L., Ge, Y., Gentry, J., et al. (2004). Bioconductor: open software development for computational biology and bioinformatics. Genome Biol. *5*, R80.

Goldberg, A.L. (2012). Development of proteasome inhibitors as research tools and cancer drugs. J. Cell Biol. *199*, 583–588.

Gomez-Pastor, R., Burchfiel, E.T., and Thiele, D.J. (2018). Regulation of heat shock transcription factors and their roles in physiology and disease. Nat. Rev. Mol. Cell Biol. *19*, 4–19.

Gonsalves, S.E., Moses, A.M., Razak, Z., Robert, F., and Westwood, J.T. (2011). Whole-genome analysis reveals that active heat shock factor binding sites are mostly associated with non-heat shock genes in Drosophila melanogaster. PLoS ONE *6*, e15934.

Guettouche, T., Boellmann, F., Lane, W.S., and Voellmy, R. (2005). Analysis of phosphorylation of human heat shock factor 1 in cells experiencing a stress. BMC Biochem. *6*, 4.

Hahn, J.-S., Hu, Z., Thiele, D.J., and Iyer, V.R. (2004). Genome-wide analysis of the biology of stress responses through heat shock transcription factor. Mol. Cell. Biol. *24*, 5249–5256.

Härmä, V., Virtanen, J., Mäkelä, R., Happonen, A., Mpindi, J.P., Knuuttila, M., Kohonen, P., Lötjönen, J., Kallioniemi, O., and Nees, M. (2010). A comprehensive panel of three-dimensional models for studies of prostate cancer growth, invasion and drug responses. PLoS ONE *5*, e10431.

Hartl, F.U., Bracher, A., and Hayer-Hartl, M. (2011). Molecular chaperones in protein folding and proteostasis. Nature *475*, 324–332.

Hayashi, S., and Takeichi, M. (2015). Emerging roles of protocadherins: from self-avoidance to enhancement of motility. J. Cell Sci. *128*, 1455–1464.

Hershko, A., and Ciechanover, A. (1998). The ubiquitin system. Annu. Rev. Biochem. *67*, 425–479.

Hirano, S., and Takeichi, M. (2012). Cadherins in brain morphogenesis and wiring. Physiol. Rev. *92*, 597–634.

Huang, W., Sherman, B.T., and Lempicki, R.A. (2009). Systematic and integrative analysis of large gene lists using DAVID bioinformatics resources. Nat. Protoc. *4*, 44–57.

Hulsen, T., de Vlieg, J., and Alkema, W. (2008). BioVenn - a web application for the comparison and visualization of biological lists using area-proportional Venn diagrams. BMC Genomics *9*, 488.

Jaeger, A.M., Pemble, C.W., 4th, Sistonen, L., and Thiele, D.J. (2016). Structures of HSF2 reveal mechanisms for differential regulation of human heat-shock factors. Nat. Struct. Mol. Biol. *23*, 147–154.

Joutsen, J., and Sistonen, L. (2019). Tailoring of Proteostasis Networks with Heat Shock Factors. Cold Spring Harb. Perspect. Biol. *11*, a034066.

Kallio, P.J., Wilson, W.J., O'Brien, S., Makino, Y., and Poellinger, L. (1999). Regulation of the hypoxia-inducible transcription factor 1α by the ubiquitin-proteasome pathway. J. Biol. Chem. *274*, 6519–6525.

Kallio, M., Chang, Y., Manuel, M., Alastalo, T.P., Rallu, M., Gitton, Y., Pirkkala, L., Loones, M.T., Paslaru, L., Larney, S., et al. (2002). Brain abnormalities, defective meiotic chromosome synapsis and female subfertility in HSF2 null mice. EMBO J. *21*, 2591–2601.

Kampinga, H.H., Hageman, J., Vos, M.J., Kubota, H., Tanguay, R.M., Bruford, E.A., Cheetham, M.E., Chen, B., and Hightower, L.E. (2009). Guidelines for the nomenclature of the human heat shock proteins. Cell Stress Chaperones *14*, 105–111.

Kawazoe, Y., Nakai, A., Tanabe, M., and Nagata, K. (1998). Proteasome inhibition leads to the activation of all members of the heat-shock-factor family. Eur. J. Biochem. *255*, 356–362.

Kim, D., Pertea, G., Trapnell, C., Pimentel, H., Kelley, R., and Salzberg, S.L. (2013). TopHat2: accurate alignment of transcriptomes in the presence of insertions, deletions and gene fusions. Genome Biol. *14*, R36.

Kisselev, A.F., Callard, A., and Goldberg, A.L. (2006). Importance of the different proteolytic sites of the proteasome and the efficacy of inhibitors varies with the protein substrate. J. Biol. Chem. *281*, 8582–8590.

Kobayashi, A., Kang, M.I., Okawa, H., Ohtsuji, M., Zenke, Y., Chiba, T., Igarashi, K., and Yamamoto, M. (2004). Oxidative stress sensor Keap1 functions as an adaptor for Cul3-based E3 ligase to regulate proteasomal degradation of Nrf2. Mol. Cell. Biol. *24*, 7130–7139.

Korfanty, J., Stokowy, T., Widlak, P., Gogler-Piglowska, A., Handschuh, L., Podkowiński, J., Vydra, N., Naumowicz, A., Toma-Jonik, A., and Widlak, W. (2014). Crosstalk between HSF1 and HSF2 during the heat shock response in mouse testes. Int. J. Biochem. Cell Biol. *57*, 76–83.

Kubbutat, M.H., Jones, S.N., and Vousden, K.H. (1997). Regulation of p53 stability by Mdm2. Nature *387*, 299–303.

Lecomte, S., Desmots, F., Le Masson, F., Le Goff, P., Michel, D., Christians, E.S., and Le Dréan, Y. (2010). Roles of heat shock factor 1 and 2 in response to proteasome inhibition: consequence on p53 stability. Oncogene *29*, 4216–4224.

Li, J., Chauve, L., Phelps, G., Brielmann, R.M., and Morimoto, R.I. (2016). E2F coregulates an essential HSF developmental program that is distinct from the heat-shock response. Genes Dev. *30*, 2062–2075.

Liao, Y., Smyth, G.K., and Shi, W. (2013). The Subread aligner: fast, accurate and scalable read mapping by seed-and-vote. Nucleic Acids Res. *41*, e108.

Ling, Y.H., Liebes, L., Ng, B., Buckley, M., Elliott, P.J., Adams, J., Jiang, J.D., Muggia, F.M., and Perez-Soler, R. (2002). PS-341, a novel proteasome inhibitor, induces Bcl-2 phosphorylation and cleavage in association with G2-M phase arrest and apoptosis. Mol. Cancer Ther. *1*, 841–849.

Mahat, D.B., Salamanca, H.H., Duarte, F.M., Danko, C.G., and Lis, J.T. (2016). Mammalian heat shock response and mechanisms underlying its genome-wide transcriptional regulation. Mol. Cell *62*, 63–78.

Mali, P., Yang, L., Esvelt, K.M., Aach, J., Guell, M., DiCarlo, J.E., Norville, J.E., and Church, G.M. (2013). RNA-guided human genome engineering via Cas9. Science *339*, 823–826.

Mathew, A., Mathur, S.K., and Morimoto, R.I. (1998). Heat shock response and protein degradation: regulation of HSF2 by the ubiquitin-proteasome pathway. Mol. Cell. Biol. *18*, 5091–5098.

Mendillo, M.L., Santagata, S., Koeva, M., Bell, G.W., Hu, R., Tamimi, R.M., Fraenkel, E., Ince, T.A., Whitesell, L., and Lindquist, S. (2012). HSF1 drives a transcriptional program distinct from heat shock to support highly malignant human cancers. Cell *150*, 549–562.

Mezger, V., Rallu, M., Morimoto, R.I., Morange, M., and Renard, J.P. (1994). Heat shock factor 2-like activity in mouse blastocysts. Dev. Biol. *166*, 819–822.

Östling, P., Björk, J.K., Roos-Mattjus, P., Mezger, V., and Sistonen, L. (2007). Heat shock factor 2 (HSF2) contributes to inducible expression of hsp genes through interplay with HSF1. J. Biol. Chem. *282*, 7077–7086.

Ozawa, M., and Kemler, R. (1998). Altered cell adhesion activity by pervanadate due to the dissociation of alpha-catenin from the E-cadherin.catenin complex. J. Biol. Chem. *273*, 6166–6170.

Peek, S.L., Mah, K.M., and Weiner, J.A. (2017). Regulation of neural circuit formation by protocadherins. Cell. Mol. Life Sci. *74*, 4133–4157.

Pirkkala, L., Alastalo, T.-P., Zuo, X., Benjamin, I.J., and Sistonen, L. (2000). Disruption of heat shock factor 1 reveals an essential role in the ubiquitin proteolytic pathway. Mol. Cell. Biol. *20*, 2670–2675.

Rallu, M., Loones, M., Lallemand, Y., Morimoto, R., Morange, M., and Mezger, V. (1997). Function and regulation of heat shock factor 2 during mouse embryogenesis. Proc. Natl. Acad. Sci. USA *94*, 2392–2397.

Ritchie, M.E., Phipson, B., Wu, D., Hu, Y., Law, C.W., Shi, W., and Smyth, G.K. (2015). limma powers differential expression analyses for RNA-sequencing and microarray studies. Nucleic Acids Res. *43*, e47.

Riva, L., Koeva, M., Yildirim, F., Pirhaji, L., Dinesh, D., Mazor, T., Duennwald, M.L., and Fraenkel, E. (2012). Poly-glutamine expanded huntingtin dramatically alters the genome wide binding of HSF1. J. Huntingtons Dis. *1*, 33–45.

Robinson, M.D., McCarthy, D.J., and Smyth, G.K. (2010). edgeR: a Bioconductor package for differential expression analysis of digital gene expression data. Bioinformatics *26*, 139–140.

Rossi, A., Riccio, A., Coccia, M., Trotta, E., La Frazia, S., and Santoro, M.G. (2014). The proteasome inhibitor bortezomib is a potent inducer of zinc finger AN1-type domain 2a gene expression: role of heat shock factor 1 (HSF1)-heat shock factor 2 (HSF2) heterocomplexes. J. Biol. Chem. *289*, 12705–12715.

Rueden, C.T., Schindelin, J., Hiner, M.C., DeZonia, B.E., Walter, A.E., Arena, E.T., and Eliceiri, K.W. (2017). ImageJ2: ImageJ for the next generation of scientific image data. BMC Bioinformatics *18*, 529.

Sarge, K.D., Zimarino, V., Holm, K., Wu, C., and Morimoto, R.I. (1991). Cloning and characterization of two mouse heat shock factors with distinct inducible and constitutive DNA-binding ability. Genes Dev. *5*, 1902–1911.

Sarge, K.D., Murphy, S.P., and Morimoto, R.I. (1993). Activation of heat shock gene transcription by heat shock factor 1 involves oligomerization, acquisition of DNA-binding activity, and nuclear localization and can occur in the absence of stress. Mol. Cell. Biol. *13*, 1392–1407.

Sarge, K.D., Park-Sarge, O.K., Kirby, J.D., Mayo, K.E., and Morimoto, R.I. (1994). Expression of heat shock factor 2 in mouse testis: potential role as a regulator of heat-shock protein gene expression during spermatogenesis. Biol. Reprod. *50*, 1334–1343.

Schindelin, J., Arganda-Carreras, I., Frise, E., Kaynig, V., Longair, M., Pietzsch, T., Preibisch, S., Rueden, C., Saalfeld, S., Schmid, B., et al. (2012). Fiji: an open-source platform for biological-image analysis. Nat. Methods *9*, 676–682.

Seong, E., Yuan, L., and Arikkath, J. (2015). Cadherins and catenins in dendrite and synapse morphogenesis. Cell Adhes. Migr. *9*, 202–213.

Shah, S.P., Nooka, A.K., Jaye, D.L., Bahlis, N.J., Lonial, S., and Boise, L.H. (2016). Bortezomib-induced heat shock response protects multiple myeloma cells and is activated by heat shock factor 1 serine 326 phosphorylation. Oncotarget *7*, 59727–59741.

Sheldon, L.A., and Kingston, R.E. (1993). Hydrophobic coiled-coil domains regulate the subcellular localization of human heat shock factor 2. Genes Dev. *7*, 1549–1558.

Shinkawa, T., Tan, K., Fujimoto, M., Hayashida, N., Yamamoto, K., Takaki, E., Takii, R., Prakasam, R., Inouye, S., Mezger, V., and Nakai, A. (2011). Heat shock factor 2 is required for maintaining proteostasis against febrile-range thermal stress and polyglutamine aggregation. Mol. Biol. Cell *22*, 3571–3583.

Sistonen, L., Sarge, K.D., and Morimoto, R.I. (1994). Human heat shock factors 1 and 2 are differentially activated and can synergistically induce hsp70 gene transcription. Mol. Cell. Biol. *14*, 2087–2099.

Stadler, M., Scherzer, M., Walter, S., Holzner, S., Pudelko, K., Riedl, A., Unger, C., Kramer, N., Weil, B., Neesen, J., et al. (2018). Exclusion from spheroid formation identifies loss of essential cell-cell adhesion molecules in colon cancer cells. Sci. Rep. *8*, 1151.

Varshavsky, A. (2012). The ubiquitin system, an immense realm. Annu. Rev. Biochem. *81*, 167–176.

Vihervaara, A., Sergelius, C., Vasara, J., Blom, M.A.H., Elsing, A.N., Roos-Mattjus, P., and Sistonen, L. (2013). Transcriptional response to stress in the dynamic chromatin environment of cycling and mitotic cells. Proc. Natl. Acad. Sci. USA *110*, E3388–E3397.

Vihervaara, A., Duarte, F.M., and Lis, J.T. (2018). Molecular mechanisms driving transcriptional stress responses. Nat. Rev. Genet. *19*, 385–397.

Vihervaara, A., Mahat, D.B., Guertin, M.J., Chu, T., Danko, C.G., Lis, J.T., and Sistonen, L. (2017). Transcriptional response to stress is pre-wired by promoter and enhancer architecture. Nat. Commun. *8*, 255.

Walter, P., and Ron, D. (2011). The unfolded protein response: from stress pathway to homeostatic regulation. Science *334*, 1081–1086.

Zhang, B., Groffen, J., and Heisterkamp, N. (2007). Increased resistance to a farnesyltransferase inhibitor by N-cadherin expression in Bcr/Abl-P190 lymphoblastic leukemia cells. Leukemia *21*, 1189–1197.

STAR★METHODS

KEY RESOURCES TABLE

REAGENT or RESOURCE	SOURCE	IDENTIFIER
Antibodies		
Rabbit polyclonal anti-GAPDH	Abcam	Cat#Ab9485; RRID:AB_307275
Rat monoclonal anti-HSC70	Enzo Life Sciences	Cat#ADI-SPA-815; RRID:AB_10617277
Rabbit polyclonal anti-HSF1	Enzo Life Sciences	Cat#ADI-SPA-901; RRID:AB_10616511
Rabbit polyclonal anti-HSF1 p326	Abcam	Cat#Ab76076; RRID:AB_1310328
Rabbit polyclonal anti-HSF2	Sigma-Aldrich	Cat#HPA031455; RRID:AB_10670702
Mouse anti-HSP70	Enzo Life Sciences	Cat#ADI-SPA-810; RRID:AB_10616513
Rabbit monoclonal anti-N-cadherin	Millipore	Cat#04-1126; RRID:AB_1977064
Rabbit polyclonal anti-N-cadherin	Abcam	Cat#Ab76057; RRID:AB_1310478
Mouse monoclonal anti-PARP-1	Santa Cruz Biotechnology	Cat#Sc-8007; RRID:AB_628105
Rabbit polyclonal anti-cleaved Caspase 3	Abcam	Cat#Ab2302; RRID:AB_302962
Mouse monoclonal anti-Pan-PCDHγA	NeuroMab	Cat#75-178; RRID:AB_2159447
Rabbit polyclonal anti-Pan-Cadherin	Abcam	Cat#Ab6529; RRID:AB_305545
Mouse monoclonal anti-Lamin A/C	Cell Signaling Technology	Cat#4777S; RRID:AB_10545756
Mouse monoclonal anti- β-tubulin	Sigma-Aldrich	Cat#T8328; RRID:AB_1844090
Mouse monoclonal anti-cleaved PARP antibody conjugated to BV421		Cat#564129; RRID:AB_2738611
Goat anti-rabbit Alexa Fluor 488	Invitrogen	Cat# R37116; RRID:AB_2556544
Chemicals, Peptides, and Recombinant Proteins		
Bortezomib	Santa Cruz Biotechnology	Cat#sc-217785
MG132	Peptide Institute Inc.	Cat#317-V
17-AAG	InvivoGen	Cat#anti-agl-5
Geldanamycin	InvivoGen	Cat#anti-gl-5
L-Canavanine sulfate salt	Sigma-Aldrich	Cat#C9758
Alexa Fluor 488 Phalloidin	Thermo Fisher Scientiffic	Cat#A12379; Cat #A22287
Critical Commercial Assays		
CellTiter-Glo reagent	Promega	Cat#G7570
Calcein AM	R&D Systems	Cat#4892-010-K
AllPrep DNA/RNA/miRNA Universal Kit	QIAGEN	Cat#80224
Matrigel	Corning	Cat#356231
RNeasy mini kit	QIAGEN	Cat#74106
iScript cDNA Synthesis Kit	Bio-Rad	Cat#1708891
GenJet	SignaGen Laboratories	Cat#SL100489-OS
Deposited Data		
RNA-seq raw data	This paper	GEO: GSE115973
Experimental Models: Cell Lines		
U2OS wild-type	This paper	N/A
U2OS HSF2 knock out	This paper	N/A
U2OS HSF2 knock out clone 2	This paper	N/A
Mouse embryonic fibroblasts wild-type	Östling et al., 2007	N/A
Mouse embryonic fibroblasts *Hsf2*$^{-/-}$	Östling et al., 2007	N/A
Experimental Models: Organisms/Strains		
Chicken: fertilized white Leghorn chicken eggs	Munax Oy	N/A

(*Continued on next page*)

Continued

REAGENT or RESOURCE	SOURCE	IDENTIFIER
Oligonucleotides		
Primers for generating HSF2 knock-out U2OS cells with CRISPR-Cas9 see Table S2	This paper	N/A
Primer RNA18S5 forward: GCAATTATTCCCCATGAACG	Sigma-Aldrich	N/A
Primer RNA18S5 reverse: GGGACTTAATCAACGCAAGC	Sigma-Aldrich	N/A
Probe RNA18S5: FAM-TTCCCAGTAAGTGCG GGTC-BHQ	Sigma-Aldrich	N/A
Primer DSC2 forward: ATCCATTAGAGGACACACTCTGA	Sigma-Aldrich	N/A
Primer DSC2 reverse: GCCACCGATCCTCTTCCTTC	Sigma-Aldrich	N/A
Primer PCDHA6 forward: TGACTGTTGAATGATGGCGGA	Sigma-Aldrich	N/A
Primer PCDHA6 reverse: TCGGGTACGGAGTAGTGGAG	Sigma-Aldrich	N/A
Primer PCDH10A forward: AGGCATCAGCCAGTTTCTCAA	Sigma-Aldrich	N/A
Primer PCDH10A reverse: GAGAGCAGCAGACACTGGAC	Sigma-Aldrich	N/A
Recombinant DNA		
pMLM3636, Human-gRNA-Expression Vector	Keith Joung laboratory, Addgene	RRID:Addgene_43860
pcDNA3.3-TOPO hCas9	Mali et al., 2013; Addgene	RRID:Addgene_41815
pEGFP-N1	Clontech	N/A
shRNA against HSF2 in pSUPERIOR	Östling et al., 2007	N/A
shRNA scrambled in pSUPERIOR	Östling et al., 2007	N/A
N-Cadherin in pCCL-c-MNDU3c-PGK-EGFP	Zhang et al., 2007; Addgene	RRID:Addgene_38153
Software and Algorithms		
FastQC version 0.20.1	Andrews, 2010; FastQC.	http://www.bioinformatics.babraham.ac.uk/projects/fastqc/
TopHat2 version 2.1.0	Kim et al., 2013	https://ccb.jhu.edu/software/tophat/index.shtml
Subreads version 1.5.0	Liao et al., 2013	
R: A language an Environment for Statistical Computing	R Core Tean	https://www.r-project.org/
Bioconductor	Gentleman et al., 2004	http://www.bioconductor.org/
Bioconductor R package edgeR	Robinson et al., 2010	https://bioconductor.org/packages/release/bioc/html/edgeR.html
Bioconductor R package Limma	Ritchie et al., 2015	https://bioconductor.org/packages/release/bioc/html/limma.html
Bioconductor R package topGO	Alexa and Rahnenfuhrer, 2019	https://bioconductor.org/packages/release/bioc/html/topGO.html
Bioconductor R package GOstats	Falcon and Gentleman, 2007	https://bioconductor.org/packages/release/bioc/html/GOstats.html
ImageJ v1.51n	Rueden et al., 2017	https://imagej.net/Citing
Fiji	Schindelin et al., 2012	https://imagej.net/Citing
3D Object Counter	Bolte and Cordelières, 2006	https://imagej.net/Citing
FlowJo	Version 10	https://www.flowjo.com/
DAVID Bioinformatic Tool	Huang et al., 2009	https://david.ncifcrf.gov/home.jsp
GraphPad Prism Software	Version 7 and 8	https://www.graphpad.com/
BioVenn	Hulsen et al., 2008	http://www.biovenn.nl

LEAD CONTACT AND MATERIALS AVAILABILITY

Further information and requests for resources and reagents should be directed to and will be fulfilled by the Lead Contact, Lea Sistonen (lea.sistonen@abo.fi). The resources are shared for research and educational purposes without restriction.

EXPERIMENTAL MODEL AND SUBJECT DETAILS

Generation of HSF2 knock-out U2OS cells with CRISPR-Cas9

Guide RNAs (gRNA) targeting the exon 1 of *HSF2* were designed using CRISPOR software (http://crispor.tefor.net/) and cloned into pMLM3636 gRNA expression plasmid (a gift from Keith Joung, Addgene plasmid #43860). Human osteosarcoma U2OS cells were transfected with Cas9 and gRNA expression plasmids using Amaxa electroporation as recommended by the manufacturer (Lonza). The hCas9 was a gift from George Church (Addgene plasmid #41815; http://addgene.org/41815; RRID:Addgene_41815). One week after transfections, cells were seeded at single cell density. Clones were genotyped by DNA sequencing of PCR products spanning the targeted region of the *HSF2* gene. The selected U2OS clones presented 3 different outframe mutations on *HSF2* exon 1, each corresponding to a different allele (Table S2). Guide RNA sequence targeting the 1st AUG of the *HSF2* exon 1: 5′-UGCGCCGC GUUAACAAUGAA-3′. Following primers were used for PCR for validation: forward (hHSF2_Cr_ATG_F): 5′-AGTCGGCTCCTGG GATTG-3′ and reverse (hHSF2_Cr_ATG_R): 5′-AGTGAGGAGGCGGTTATTCAG-3′. For the experiments, we utilized HSF2 knock-out cell clone 1 (hereafter 2KO) and HSF2 knock-out cell clone 2 (hereafter 2KO#2).

Cell culture

U2OS cells and mouse embryonic fibroblasts (WT and *Hsf2*$^{-/-}$ MEFs, Östling et al., 2007) were cultured in DMEM (Dulbecco's Modified Eagle's media, D6171, Sigma-Aldrich), supplemented with 10% fetal calf serum, 2 mM L-glutamine and 100 μg/ml penicillin-streptomycin, and grown in 5% CO_2 at 37°C. Culture media for MEFs were also supplemented with 1 X MEM non-essential amino acid solution (M7145, Sigma-Aldrich).

Chicken chorioallantoic membrane (CAM) assay

The CAM-assay was performed as in Björk et al. (2016). Briefly, fertilized white Leghorn chicken eggs were incubated at 37°C under 60% humidity (embryo development day 0, EDD0). Separation of the developing CAM was induced on EDD4. On EDD8, 1 × 10^6 U2OS WT and 2KO cells were mixed with Matrigel in 1:1 ratio and implanted on the CAM. On EDD11, the tumors were photographed *in ovo*. Tumor area was measured in blind using ImageJ.

METHOD DETAILS

Treatments

Proteasome inhibition was induced with Bortezomib (BTZ, sc-217785, Santa Cruz Biotechnology) or MG132 (Z-Leu-Leu-Leu-H, 317-V, Peptide Institute Inc.). For HSP90 inhibition, 17-AAG (anti-agl-5, InvivoGen) and Geldanamycin (anti-gl-5, InvivoGen) were used. All inhibitors were diluted in DMSO (dimethyl sulfoxide, D8418, Sigma-Aldrich) and applied to cells in final concentrations indicated in the figures. Control cells were treated with DMSO only. To induce protein misfolding with amino acid analogs, cells were starved for 17 h in L-arginine free culture medium (A14431-01, GIBCO) supplemented with 10% fetal calf serum, 2 mM L-glutamine and 100 μg/ml penicillin-streptomycin. Following that, L-Canavanine sulfate salt (C9758, Sigma-Aldrich) was applied to the cells in final concentrations indicated in the figure. Cells were treated for 3 or 6 h. After the treatments, cells were visualized with Leica phase contrast microscope, an EVOS FL Cell Imaging System (Thermo Fisher Scientific), or an Axio Vert A1-FL LED microscope (Carl Zeiss) and harvested for further analyses.

Transfections

For transfections, 6 × 10^6 U2OS WT or 2KO cells were suspended in 400 μL of Opti-MEM (11058-021, GIBCO) and subjected to electroporation (230 V, 975 μF) in BTX electroporation cuvettes (45-0126, BTX). To downregulate HSF2 in WT cells, HSF2 targeting shRNA and Scr vectors as previously described (Östling et al., 2007), were used. For restoring the protein levels of HSF2 and N-Cadherin in 2KO cells, HSF2 in pcDNA3.1/myc-His(-)A vector and N-cadherin in pCCL-c-MNDU3c-PGK-EGFP (Zhang et al., 2007) (a gift from Nora Heisterkamp; Addgene plasmid #38153; http://addgene.org/38153; RRID:Addgene_38153) were used. Empty pcDNA3.1/myc-His(-)A vector was used as Mock. One day after transfection, cells were trypsinized, counted, re-plated, and let to recover for 24 h before BTZ treatments.

For cell aggregation assays, cells were transfected with GenJet (#SL100489-OS, SignaGen Laboratories) according to manufacturer's instructions. Briefly, cells were plated 18 to 24 h prior to transfections to ensure 80% confluency, and fresh culture media with supplements was added to the cells before transfections. The N-Cadherin encoding vector (described above) was used for transfections, and pEGFP-N1 (Clontech) was used as a Mock. The plasmids and the GenJet reagent were diluted in serum free media, and applied to the cells in a ratio of 1:2 (DNA:GenJet reagent). Cells were incubated with the DNA:GenJet mixture for 4 h, washed with PBS, and supplemented with complete culture media. Cells were let to recover for 24 h before the cell aggregation experiments.

Immunoblotting

Cells were collected in culture media, washed with PBS (L0615, BioWest) and lysed in lysis buffer [50 mM HEPES, pH 7.4, 150 mM NaCl, 1 mM EDTA, 2 mM $MgCl_2$, 1% Triton X-100, 10% glycerol, 1 x complete Protease Inhibitor Cocktail (04693159001, Roche Diagnostics), 50 mM NaF, 0.2 mM Na_3VO_4]. Protein concentration of the lysates was determined with Bradford assay. Equal amounts

of cell lysates were resolved on 4%–20% or 7.5% Mini-PROTEAN® TGX precast gels (Bio-Rad) and the proteins were transferred to a nitrocellulose membrane. For HSF2 detection, membranes were boiled for 15 min in MQ-H_2O and blocked in 3% milk-PBS-Tween20 solution for 1 h at RT. Primary antibodies were diluted in 0.5% BSA-PBS-0.02% NaN_3 and the membranes were incubated in respective primary antibodies overnight at 4°C. The following antibodies were used: anti-GAPDH (ab9485, Abcam), anti-HSC70 (ADI-SPA-815, Enzo Life Sciences), anti-HSF1 (ADI-SPA-901, Enzo Life Sciences), anti-HSF1 pS326 (ab76076, Abcam), anti-HSF2 (HPA031455, Sigma-Aldrich), anti-HSP70 (ADI-SPA-810, Enzo Life Sciences), N-cadherin (04-1126, Millipore or ab76057, Abcam), anti-PARP-1 (F-2, sc-8007, Santa Cruz Biotechnology), anti-Caspase-3 (ab2302, Abcam), anti-Pan-PCDHγA (75-178, NeuroMab), anti-Pan-Cadherin (ab6529, Abcam), anti-Lamin A/C (4777S, Cell Signaling Technology), and anti-β-Tubulin (T8328, Sigma-Aldrich). Secondary antibodies were HRP-conjugated and purchased from Promega, GE Healthcare or Abcam. All immunoblotting experiments were performed at least three times.

Immunofluorescence

2×10^5 U2OS WT cells were plated on coverslips or MatTek plates (P35GC-.5-14-C, MatTek Corporation) 24 h before treatments. Cells were fixed with 4% paraformaldehyde (PFA) for 15 min, permeabilized in 0.1% Triton X-100 in PBS and washed three times with PBST (PBS-0.5% Tween20). Cells were blocked with 10% FBS in PBS for 1 h at RT and incubated overnight at 4°C with a primary anti-HSF2 antibody (HPA031455, Sigma-Aldrich), which was diluted 1:20 in 10% FBS-PBS. Secondary goat anti-rabbit Alexa Fluor 488 (R37116, Invitrogen) was diluted 1:500 in 10% FBS-PBS and the cells were incubated for 1 h in RT. Cells were washed three times with PBST, incubated with 300 nM DAPI diluted in PBS or mounted in Mowiol-DABCO or VECTASHIELD mounting medium, and imaged with a 3i CSU-W1 spinning disc confocal microscope (Intelligent Imaging Innovations).

Subcellular fractionation

2×10^6 U2OS WT cells were plated and cultured overnight. The following day, cells were treated with 25 nM BTZ for 6 or 22 h. Control cells were treated with DMSO for 22 h. Cells were collected in culture media and washed with PBS. 20% of the suspended cells were collected for preparation of the whole cell lysate and lysed. The remaining 80% were collected for subcellular fractionation. Cytoplasmic and nuclear fractions were prepared using NE-PER Nuclear and Cytoplasmic Extraction Reagents (78833, Thermo Fisher Scientific) according to manufacturer's instructions. Briefly, suspended cells were washed with cold PBS. The cell pellet was suspended in 200 μL of cytoplasmic extraction reagent I. After incubation on ice, 11 μL of cytoplasmic extraction reagent II was added. The suspension was incubated on ice and centrifuged (16 000 g, 5 min). The supernatant was collected and the pellet was resuspended in 100 μL of nuclear extraction reagent, incubated on ice and centrifuged (16 000 g, 10 min). The supernatant (nuclear extract) was collected and the protein concentrations were determined by BCA assay (23225, Thermo Fischer Scientific).

Cell viability measurements

5×10^3 U2OS WT and HSF2 KO cells were cultured in clear bottom 96-well plate (6005181, Perking Elmer) in complete culture media. Cells were treated with indicated concentrations of Bortezomib or MG132 for 22 h. For calcium-depletion, cells were treated with or without 25 nM BTZ (U2OS cells) or 5 and 10 nM BTZ (MEFs) for 20 h in serum free media. The extracellular calcium was depleted with 4 mM EGTA (U2OS cells) and 2 mM EGTA (MEFs) in calcium-free media and the Bortezomib treatment was continued for 2 h. Control cells were treated with DMSO. After treatments cells were washed with PBS and incubated for 30 min at 37°C with Calcein AM (4892-010-K, R&D Systems) diluted 1:1000 in PBS. Fluorescence intensity was measured with Hidex Sense microplate reader (HIDEX Corp) with excitation and emission wavelengths 485 nm and 535 nm, respectively. Alternatively, CellTiter-Glo reagent (G7570, Promega) was added to the wells in 1:1 ratio and the luminescence was measured with Hidex Sense microplate reader. Respective blank values were subtracted from the sample values and the viability of untreated control samples was set to value 1. All measurements were repeated at least three times.

Cell aggregation assays

After trypsinization, 5×10^5 U2OS WT and 2KO cells were suspended in 2 mL of aggregation assay buffer (137 mM NaCl, 5.4 mM KCl, 0.63 mM, Na_2HPO_4, 5.5 mM glucose, and 10 mM HEPES, pH 7.4) supplemented with either 3 mM $CaCl_2$ or 3 mM EDTA. Cells were rotated for 2.5 h in 150 rpm at 37°C, after which the aggregates were imaged with the EVOS FL Cell Imaging System (Thermo Fisher Scientific) or with an Axio Vert A1-FL LED microscope (Carl Zeiss). Cell aggregation assays were performed in biological triplicates. The area of the three biggest aggregates in each sample was measured with ImageJ (U. S. National Institutes of Health, Bethesda, Maryland, USA) for quantification purposes. All cell aggregation experiments were repeated at least three times.

RNA-sequencing

2×10^6 U2OS WT and HSF2 KO cells were plated and cultured overnight. Following day, cells were treated with 25 nM BTZ for 6 or 10 h. Control cells were treated with DMSO. Cells were collected, and total RNA was purified with AllPrep DNA/RNA/miRNA Universal Kit (80224, QIAGEN) according to manufacturer's instructions. Genomic DNA from mRNA columns was digested with DNase I. The RNA library was prepared according to Illumina TruSeq® Stranded mRNA Sample Preparation Guide (part #15031047). Briefly, poly-A containing mRNA molecules were purified with poly-T oligo magnetic beads and fragmented with divalent cations under elevated temperatures. For first-strand cDNA synthesis, RNA fragments were copied using reverse transcriptase and random

primers. Unique Illumina TrueSeq indexing adapters were ligated to each sample. The quality and concentration of cDNA samples were analyzed with Advanced Analytical Fragment Analyzer and Bioanalyzer 2100 (Agilent, Santa Clara, CA, USA) and Qubit® Fluorometric Quantitation (Life Technologies). Samples were sequenced with Illumina HiSeq 3000 (Illumina). All the experimental steps after the RNA extraction were conducted in the Finnish Microarray and Sequencing Center, Turku, Finland. RNA-sequencing was performed from four independent sample series.

Flow cytometry

0.5×10^6 U2OS WT and 2KO cells were fixed at 4°C with BD Cytofix/Cytoperm (554722, BD Bioscience) and washed with cold BD Perm/Wash (554723, BD Bioscience) solution. Cells were incubated over night at 4°C with anti-cleaved PARP antibody conjugated to BV421 (564129, BD Horizon), which was diluted 1:250 in BD Perm/Wash solution. Fluorescence was analyzed with a BD LSRFortessa flow cytometer (BD Bioscience) using a standard Pacific Blue filter set (450/50 nm). The flow cytometry profiles were analyzed using FlowJo 10 software.

Quantitative RT-PCR (qRT-PCR)

RNA was isolated using a RNeasy mini kit (74106, QIAGEN) according to the manufacturer's instructions and quantified using a NanoDrop ND-1000 spectrophotometer (Thermo Fisher Scientific). Following that, 1 μg of total RNA was reverse transcribed with an iScript cDNA Synthesis Kit (#1708891, Bio-Rad). SensiFAST Probe Lo-ROX and SensiFAST SYBR® Lo-ROX kits (Bioline) were used for qRT-PCRs that were performed with QuantStudio 3 Real-Time PCR system (Applied Biosystems, Thermo Fisher Scientific). All primers and probes were purchased from Sigma Aldrich. The following forward (f) and reverse (r) primers, and probes (pr) were used: fRNA18S5, 5′-GCAATTATTCCCCATGAACG-3′; rRNA18S, 5′- GGGACTTAATCAACGCAAGC-3′; prRNA18S5, 5′-FAM-TTCCCAGTAAGTGCG GGTC-BHQ-3′; fDSC2; 5′-ATCCATTAGAGGACACACTCTGA-3′; rDSC2, 5′- GCCACCGATCCTCTT CCTTC-3′; fPCDHA6, 5′-TGACTGTTGAATGATGGCGGA-3′; rPCDHA6, 5′-TCGGGTACGGAGTAGTGGAG-3′; fPCDHA10, 5′- AGG CATCAGCCAGTTTCTCAA-3′; rPCDHA10, 5′-GAGAGCAGCAGACACTGGAC-3′. The mRNA expression levels were normalized against the respective 18S RNA (*RNA18S5*) expression in a given sample. All reactions were run in triplicate from samples derived from four biological replicates.

3D cell culture and immunofluorescence

5×10^3 U2OS WT and 2KO cells were cultured on Clear Round Bottom Ultra-Low Attachment (ULA) Microplates (#7007, Corning). 1×10^6 cells were used for bacterial plates. After 24 and 48 h, cells were imaged with Axio Vert A1-FL LED microscope (Carl Zeiss). For 3D in Matrigel, cells were embedded in growth factor reduced Matrigel (#356231, Corning) and cultured in Angiogenesis μ-slides (#81501, Ibidi) as described previously (Härmä et al., 2010). Briefly, wells were filled with 10 μl of Matrigel:culture medium (1:1 ratio), which was polymerized at 37°C for 60 min. WT, 2KO, or 2KO#2 cells were seeded on top of the gel at a density of 700 cells per well, let to attach at 37°C for 2 h, and covered with 20 μl of Matrigel:culture medium (1:4 ratio). The upper layer of Matrigel:culture medium was polymerized at 37°C overnight, and appropriate humidity was ensured by adding droplets of MQ-H_2O between the wells. Culture medium was changed every second day, and cell growth was monitored by imaging the cultures with a Zeiss Axio Vert A1-FL LED microscope (Carl Zeiss).

For immunofluorescence, spheroids were washed with 40 μl of PBS and fixed with 25 μl of 4% PFA for 20 min at RT, followed by three washes with 40 μl of PBS. Spheroids were stained with 25 μl of 0.7% Triton X-100, 1:500 Alexa Fluor 488 Phalloidin (#A12379, #A22287, Thermo Fisher Scientific), 300 nM DAPI in PBS at RT for 1 h. The stained spheroids were stored in PBS at 4°C until imaging. The spheroids were imaged as z stacks with a 3i CSU-W1 spinning disc confocal microscope (Intelligent Imaging Innovations) using the same settings between the repeats. Spheroid volume was calculated based on the phalloidin staining using ImageJ v1.51n (Rueden et al., 2017) software with the 3D Object Counter v2.0 (Bolte and Cordelières, 2006) plugin. The threshold for background and object voxels were manually adjusted for each image in order to capture the whole volume of each spheroid.

Visualization of the data

Heatmaps were generated with GraphPad Prism 7 Software (GraphPad Prism Software, La Jolla California USA, https://www.graphpad.com). Venn diagrams were generated with BioVenn web application (http://www.biovenn.nl/). DAVID Bioinformatic Resources 6.7 (https://david-d.ncifcrf.gov/home.jsp) was used for functional annotation clustering.

QUANTIFICATION AND STATISTICAL ANALYSIS

Bioinformatic analysis of the RNA-seq data

The quality of the raw sequencing reads was confirmed with FastQC version 0.20.1 and aligned against the hg38 human genome assembly using TopHat2 version 2.1.0. Subreads version 1.5.0 was used to calculate gene level expression counts according to RefSeq-based gene annotations. The downstream analysis was carried out with R and Bioconductor. The data were normalized with TMM normalization method on the edgeR package. In all sample groups, the Spearmaṅs correlation value was above 0.97, indicating high reproducibility. Statistical testing between the sample groups was carried out using Bioconductor R package Limma (Ritchie et al., 2015) and the differentially expressed genes were filtered using fold change ≥ 3 and false discovery rate (FDR) of

0.001 as cutoff. Enrichment analysis for the differentially expressed (DE) filtered genes was performed with topGO and GOstats packages. GO terms in each comparison pair were ranked according to their significance (lowest p value) and the most significantly changed terms were selected for the figures. Additional information regarding the term IDs can be found from http://geneontology.org.

Other data analyses

Statistical analyses were performed with GraphPad Prism 7 and 8 Software (GraphPad Prism Software, La Jolla California USA, https://www.graphpad.com). The statistical significance was analyzed with two-way ANOVA and Holm-Sidak's post hoc test unless indicated differently. For details, see Figures 1, 2, 3, 4, 5, and 6.

DATA AND CODE AVAILABILITY

The original data are available at Gene Expression Omnibus (GEO) database under accession number GSE115973.